Perturbation of cortical excitability in a conditional model of PCDH19 disorder

Didi Lamers
Institute Nanoscience CNR and Scuola Normale Superiore Pisa https://orcid.org/0000-0001-5539-9870

Silvia Landi
Istituto di Neuroscienze, Consiglio Nazionale delle Ricerche (CNR), Pisa, 56124 Pisa, Italy

Roberta Mezzena
Institute Nanoscience CNR and Scuola Normale Superiore Pisa

Laura Baroncelli
Department of Developmental Neuroscience, IRCCS Stella Maris Foundation

Vinoshene Pillai
National Enterprise for nanoScience and nanoTechnology (NEST), Istituto Nanoscienze, Consiglio Nazionale delle Ricerche (CNR) and Scuola Normale Superiore Pisa https://orcid.org/0000-0001-7350-3969

Federica Cruciani
National Enterprise for Nanoscience and Nanotechnology (NEST), Istituto Nanoscienze Consiglio Nazionale delle Ricerche (CNR) and Scuola Normale Superiore Pisa, 56127 Pisa

Sara Migliarini
Università di Pisa

Sara Mazzoleni
Istituto di Neuroscienze, Consiglio Nazionale delle Ricerche (CNR), Department of Medical Biotechnology and Translational Medicine (BIOMETRA), University of Milan

Massimo Pasqualetti
University of Pisa https://orcid.org/0000-0002-0844-8139

Maria Passafaro
Istituto di Neuroscienze, Consiglio Nazionale delle Ricerche (CNR), Department of Medical Biotechnology and Translational Medicine (BIOMETRA), University of Milan

Silvia Bassani
Istituto di Neuroscienze, Consiglio Nazionale delle Ricerche (CNR), Department of Medical Biotechnology and Translational Medicine (BIOMETRA), University of Milan

Gian Michele Ratto (gianmichele.ratto@sns.it)
Institute Nanoscience CNR and Scuola Normale Superiore Pisa https://orcid.org/0000-0001-9632-7769

Article

Keywords: PCDH19 Epilepsy, Girls Clustering Epilepsy, Autism Spectrum Disorder, Slow Wave Activity, Excitation: Inhibition ratio, NREM sleep, Epilepsy

Posted Date: March 22nd, 2022

DOI: https://doi.org/10.21203/rs.3.rs-1435434/v1

Perturbation of cortical excitability in a conditional model of PCDH19 disorder

Didi Lamers[1], Silvia Landi[2], Roberta Mezzena[1], Laura Baroncelli[3], Vinoshene Pillai, Federica Cruciani[1], Sara Migliarini[4], Sara Mazzoleni[5], Massimo Pasqualetti[4], Maria Passafaro[5], Silvia Bassani[5], Gian Michele Ratto[1, 6, *]

[1] National Enterprise for nanoScience and nanoTechnology (NEST), Istituto Nanoscienze, Consiglio Nazionale delle Ricerche (CNR) and Scuola Normale Superiore Pisa, 56127 Pisa, Italy;
[2] Istituto di Neuroscienze, Consiglio Nazionale delle Ricerche (CNR), Pisa, 56124 Pisa, Italy;
[3] Department of Developmental Neuroscience, IRCCS Stella Maris Foundation, I-56128, Pisa, Italy.
[4] Department of Biology, Unit of Cellular and Developmental Biology, University of Pisa, 56127 Pisa, Italy
[5] Istituto di Neuroscienze, Consiglio Nazionale delle Ricerche (CNR), Department of Medical Biotechnology and Translational Medicine (BIOMETRA), University of Milan, 20129 Milan, Italy
[6] Lead contact
[*] Correspondence: gianmichele.ratto@sns.it

Keywords

PCDH19 Epilepsy; Girls Clustering Epilepsy; Autism Spectrum Disorder; Slow Wave Activity; Excitation: Inhibition ratio; NREM sleep; Epilepsy

Abstract (150 w max)

PCDH19 epilepsy (DEE9) is an X linked epilepsy syndrome associated to cognitive and behavioural disturbances. Unlike in most other X linked diseases, heterozygous females are affected while hemizygous males are spared. It has been proposed that DEE9 pathogenesis is related to disturbed cell-to-cell communication associated with mosaicism and consequential erroneous network wiring. However, the effects of mosaic PCDH19 expression on cortical network activity are unknown. We mimicked the pathology of DEE9 by introducing a patch of mosaic protein expression in the cortex of conditional PCDH19 knockout mice. LFP recordings demonstrate transient episodes of hyperexcitability and disturbed slow wave activity – a crucial component of NREM sleep. These alterations were also observed if the mosaic patch was introduced in adult mice, demonstrating that PCDH19 is not merely a developmental disease. Our results indicate that a focal mosaic mutation of PCDH19 disrupts network cortical computation and broaden our current understanding of DEE9.

Introduction

PCDH19 epilepsy (Developmental and Epileptic Encephalopathy 9, DEE9 OMIM # 300088) is an epileptic encephalopathy likely to be the second most frequent genetic cause of epilepsy[1] in females, and it is associated with intellectual disability, autism spectrum disorder (ASD)[2–4] and late-onset schizophrenia[5]. Seizures originate early in infancy and can be focal or generalized, usually occurring in clusters[6,7]. Epilepsy ameliorates with adolescence[6], while behavioural disturbances become the most prominent feature of the disease[4].

The syndrome is caused by mutations in the X-linked gene Protocadherin 19 (*Pcdh19*)[8]. The pattern of inheritance of PE is highly unusual: unlike in most X-linked disorders, heterozygous females are severely affected while hemizygous males are spared[8]. Heterozygous females, due to random X inactivation, express the protein in a mosaic and this mosaicism underlies the phenotype of the disease. Indeed, males with somatic mutations – unlike fully mutant males - have been shown to display a phenotype[3,9,10].

Protocadherins have been implicated in circuit formation and maintenance, cell-cell adhesion, synaptic connectivity, plasticity, and cell signalling. PCDH19 is mainly expressed in the hippocampus and layers II/III and V of the cortex[8,11–13]. Since PCDH19 is present in synapses[11–13] and regulates $GABA_A$ related inhibition [14,15,] it is likely important for synapse formation and function. A cellular interference hypothesis has been proposed[3], whereby the co-existence of wild-type and knockout neurons interferes with normal cell-to-cell communication, possibly because of the interaction between PCDH19 and N-cadherin disrupts synaptic targeting leading to impaired synaptic plasticity[13].

A few mouse models of PE have been characterised, and these studies have offered support for the notion that PCDH19 regulates cell adhesion and network formation. Although no gross morphological abnormalities of cortex or hippocampus were found, these tissues displayed a peculiar pattern with PCDH19 positive and negative neurons present in separate patches[11,12], thus depicting a picture of PCDH19 as a regulator of network formation and maintenance. An important recent study outlined the presence of a considerable impairment of hippocampal circuitry[13]. At present, it is unknown whether also cortical network wiring and computation are affected by mosaic PCDH19 expression. Here, we aim to answer this question using *in vivo* electrophysiological and imaging studies in a novel mouse model of the disease. Local field potential (LFP) recordings in anesthetized animals demonstrated transient episodes of hyperexcitability and disrupted slow wave activity (SWA) in mosaic PCDH19 patches in the brain. These phenotypes were observed even if the mosaicism was introduced in adult mice, suggesting that the gene is also important for network maintenance and homeostasis. Finally, we demonstrated that network activity in mosaic tissue is shaped by low synaptic coupling, an increased excitatory to inhibitory ratio, and an increased variability of neuronal activity with a sizable population of hyperactive neurons that might trigger episodes of epileptiform activity.

Results

Creation of a focal model of mosaic PCDH19 expression

We created a patch of mosaic PCDH19 expression by injecting an AAV expressing EGFP-Cre recombinase in the right occipital cortex of a conditional mouse where exon 3 of the murine gene is flanked by a pair of LoxP sequences (figure 1A, figure S1). The opposite hemisphere was not injected and acted as an internal control. The control group was obtained by injecting an EGFP AAV in floxed littermates or an EGFP-Cre AAV in non-floxed littermates. This procedure created two coexistent types of mosaicism: a large patch of brain tissue around the injection site with a reduced PCDH19 expression surrounded by tissue with normal PCDH19 expression, and - within this patch - a mosaic of cells transduced by the virus that are likely PCDH19 negative and wild-type cells that have not been transduced by the virus. We confirmed the reduction of PCDH19 by quantitative Western Blot and in situ hybridization (figure S1).

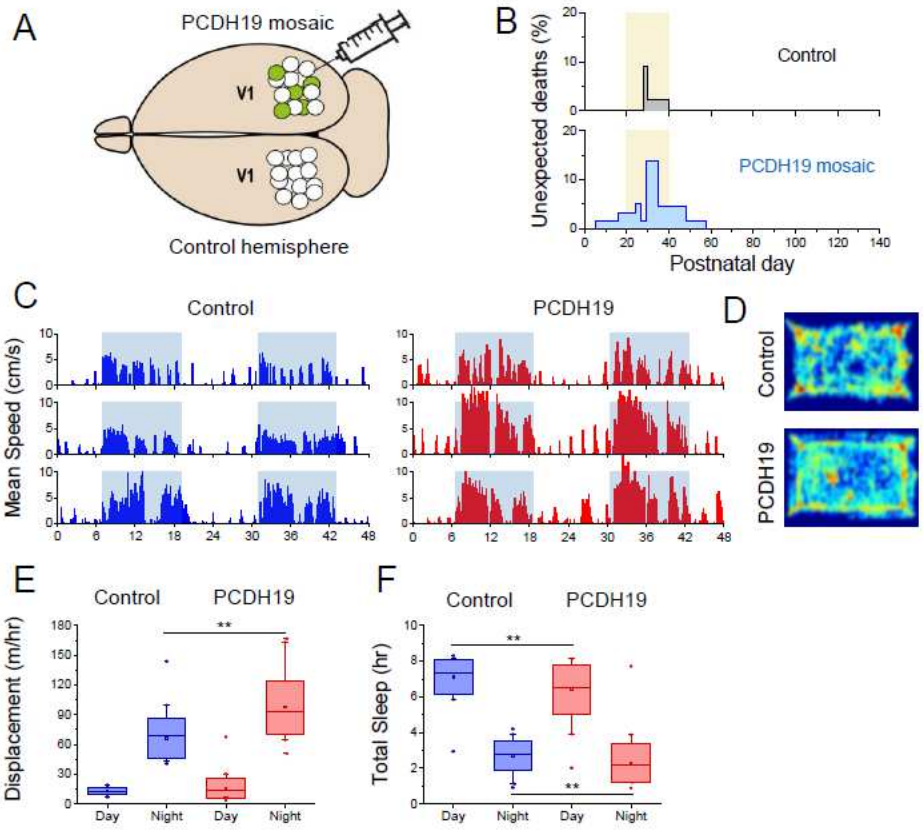

Figure 1. A) *A focal mosaic of PCDH19 expression was created by injecting an AAV expressing EGFP-Cre recombinase in the right visual cortex (V1) of the PCDH19$^{flox/flox}$ mouse. The opposite, non-injected, hemisphere was used as internal control.* ***B)*** *PCDH19 mosaic mice experienced a transient period of unexpected mortality. Data collected from 70 mice injected at P1 (blue) differs significantly from that of control littermates (48 mice, black; Mantel-Cox test P<0.01). Yellow area indicates the period of adolescence in mice.* ***C)*** *PCDH19 mice have a normal diurnal alternation of resting phases during the day (light on) and of high locomotor activity during the night (light off, shaded area; darkness from 7 PM till 7 AM). Bars represent the speed averaged in 5 min bins measured in three control and three PCDH19 mice in a 48-hour period. Recordings start at 12 AM.* ***D)*** *Density maps showing the arena occupation during a 2-hr period of the active phase.* ***E)*** *PCDH19 mice are hyperactive during the night phase.* ***F)*** *PCDH19 mice spend less time than controls in resting states that can be ascribed to sleep (n=8 for both control and PCDH19 mice; data pooled from 36 and 38 days of video recording). Significant differences are indicated with asterisks (* P<0.02, Mann Whitney test).*

Behavioural phenotype of PCDH19 mosaic mice

Mosaic mice injected at P1 showed a significant number of unexpected deaths compared to that of their control littermates (figure 1B; P<0.01) between P20 and P40, the period corresponding to early and middle adolescence in mice[16]. We tested behaviour of PCDH19 mosaic mice (P60-90) and age-matched controls by automated video recordings in an open field arena. Mice were placed in the arena at midday and, after 24 hrs of habituation, they were monitored for a period of several days in a quiet environment. First, we observed that injected mice had a normal activity pattern with most of resting during the day (light on) and higher activity during night (figure 1C). However, PCDH19 mosaic mice showed a hyperactive behaviour characterised by enhanced locomotion at night and reduced sleep (figures 1D, E, F). This macroscopic phenotype of the focal mosaic mice is particularly interesting as we disrupted PCDH19 expression in only a small patch of brain tissue, not in the entire brain.

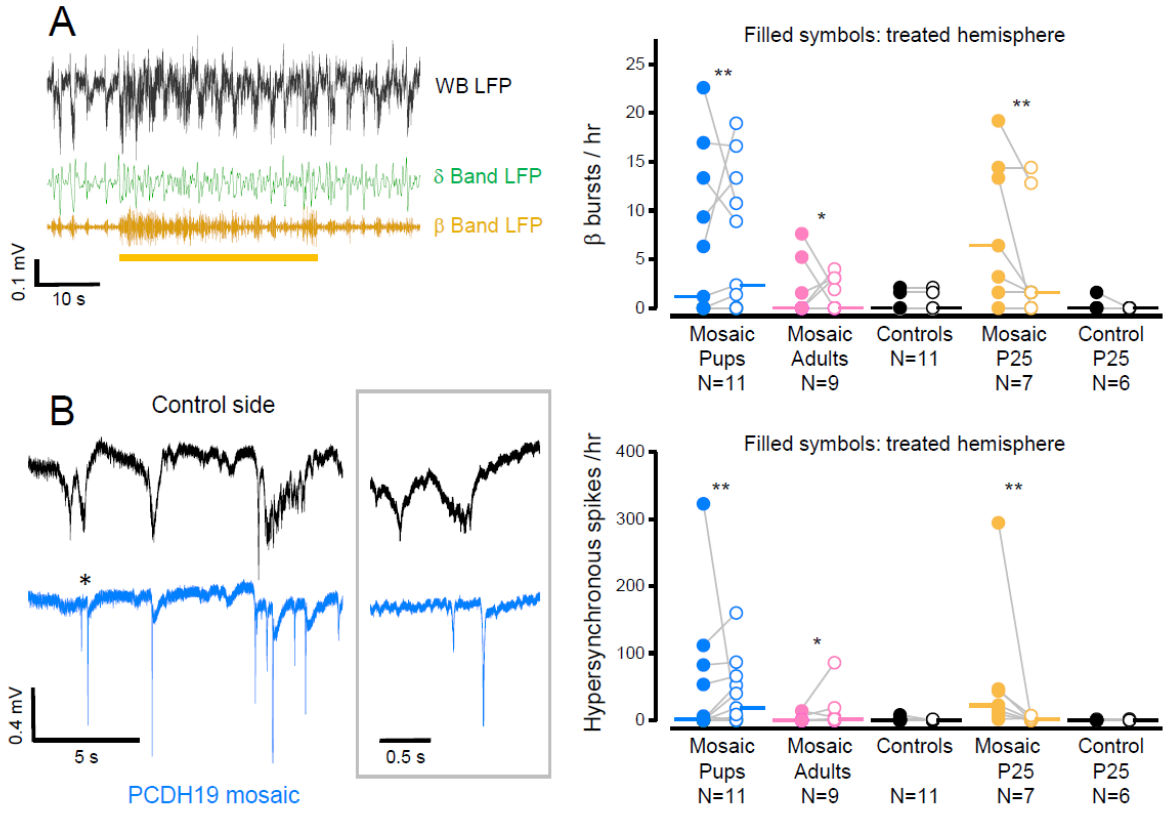

Figure 2. Hyperexcitability of the PCDH19 mosaic. A) *Left: example of a burst in the θ/σ (9-25 Hz) frequency band of the LFP recorded in the PCDH19 mosaic. The burst (yellow bar) affects the physiological slow waves as shown by the band-passed signals in the δ (0.5-4 Hz, green trace) and θ/σ (yellow) bands. Right: Number of θ bursts per hour of all recorded animals. In this and following figures, the dots represent the average value of each animal, and the lines connect corresponding data from the control and injected side (empty and filled symbols, respectively). The medians of each group are represented by horizontal lines (median>0, ** P<0.002, * P<0.02, Wilcoxon signed rank test).* ***B)*** *Left: The LFP recorded in the injected hemisphere of a mosaic pup (blue trace) shows hypersynchronous spikes while the control hemisphere (black) exhibits relatively normal SWA. The inset shows the first two peaks indicated by the asterisk). Right: Number of hypersynchronous spikes (see Materials and Methods for definition) per hour of all recorded animals (median > 0, ** P<0.002, * P<0.01, Wilcoxon signed rank test).*

Hyperexcitability of PCDH19 mosaic mice

We recorded local field potentials (LFP) from layers II/III of the occipital cortex in anesthetised mice. The most prominent feature of LFP was slow wave activity (SWA) in the δ (0.5-4 Hz) frequency band, a hallmark of deep sleep in mice and humans preserved under urethane anaesthesia[17,18].

SWA consists of 'up states' (US), characterised by neuronal depolarization and high firing activity, and 'down states' (DS) characterised by network silence[17,18]. Over imposed on this pattern, we often observed signs of a hyperexcitable phenotype in the form of sustained oscillations in the β (9-25 Hz) frequency band (figure 2A) that occurred irrespective of the phase of the δ oscillations, while, in controls, hardly any firing occurred during DSs[17,18]. Interestingly, epileptiform bursts of similar morphology were observed in a model of focal cortical dysplasia caused by the localized ablation of the gene PTEN[19]. These events occurred more frequently than 3 bursts per hour in mice injected at P1 and recorded at around P25, (5 out of 7 mice, figure 2A) and in mice recorded at P60 (5 out of 11 mice). Only a few controls (3 out of 17 mice) exhibited any β burst at all and all at a frequency lower that 2 bursts per hour, while in PCDH19 mosaics occurred at a frequency of 3 to 23 episodes per hour. This activity was observed in both hemispheres (figure 2A), thus suggesting the interhemispheric propagation of the hyperactive bursts beyond the area carrying the mutation. Importantly, even mice injected as adults showed a similar phenotype, though milder than that of mice injected at P1 (4 out of 9 exhibited more than 3 β bursts per hour).

A second form of hyperexcitability is manifested by large amplitude peaks reminiscent of interictal spikes[20,21] (figure 2B, left). Their amplitude and brief duration are indicative of hypersynchronous neuronal activity. Such events were observed in 5 out of 7 mice recorded at P25 and in 5 out of 11 mice recorded at P60. The frequency of this activity ranged from 53 to 323 peaks per hour in the injected hemisphere (figure 2B; right) and peaks had an average duration of 0.23±0.004 seconds and an amplitude of 0.49±0.09 mV. Of the 4 mice recorded at P60 that displayed peaks, 3 also displayed β oscillations. Interestingly, 81±8% of all the observed peaks occurred while the control hemisphere was in an US (significantly more than chance, one sample t test $P<0.05$, see the example in figure 2B left). Such a phase locking of hypersynchronous spikes to USs has also been shown for interictal spikes evoked by the $GABA_A$ competitive antagonist bicuculline[22]. Importantly, hypersynchronous peaks also occurred in mice injected as adults (figure 2B; right), thus suggesting that PE may not merely be a developmental disease and that the gene has a function also later in life.

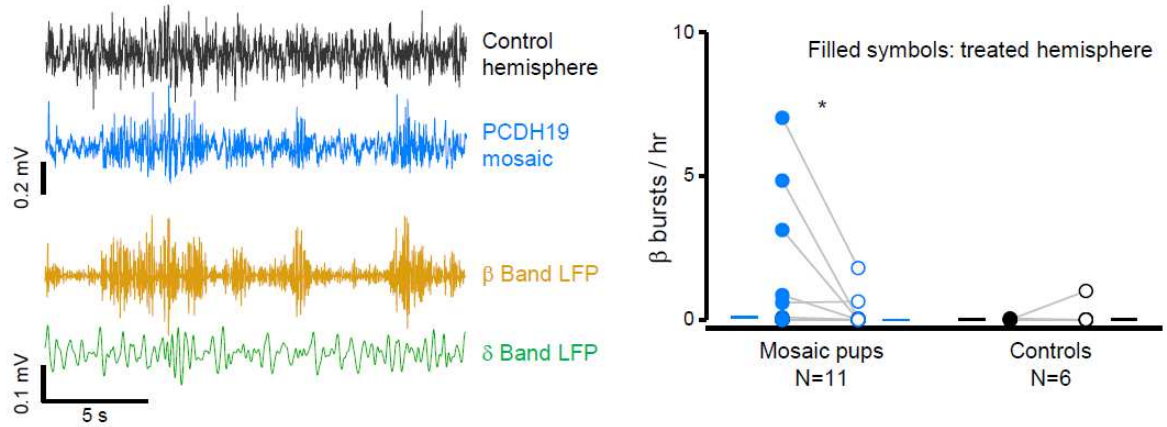

Figure 3. β bursts in the EEG of freely behaving mice. *Left: example of oscillations in the β frequency band in EEG recordings. Notice how the oscillations are better defined in the injected hemisphere (blue trace) than in the control hemisphere (black). In this example, the burst in the 9-25 Hz range (yellow) occurs during a period of prominent δ oscillations (green), indicating that the mouse is sleeping (see Materials and Methods for sleep scoring). Right: Number of β bursts per hour. Of the 11*

*recorded mice, 3 displayed more than 1 oscillations per hour (median > 0, * P<0.01, Wilcoxon signed rank test).*

The β-band bursts also occurred in behaving mice, as shown by chronic EEG recordings performed for at least 24 hours. Transient oscillations in the β band were frequently observed in mice that were injected at P1 and recorded as young adults (figure 3). Of the 11 recorded mice, 3 showed frequent bursts. Interestingly, 87% (significantly more than chance, one sample t test P<0.01) of the β-oscillations in the injected hemisphere of mosaic animals occurred during NREM sleep, suggesting a coupling of this activity to SWA.

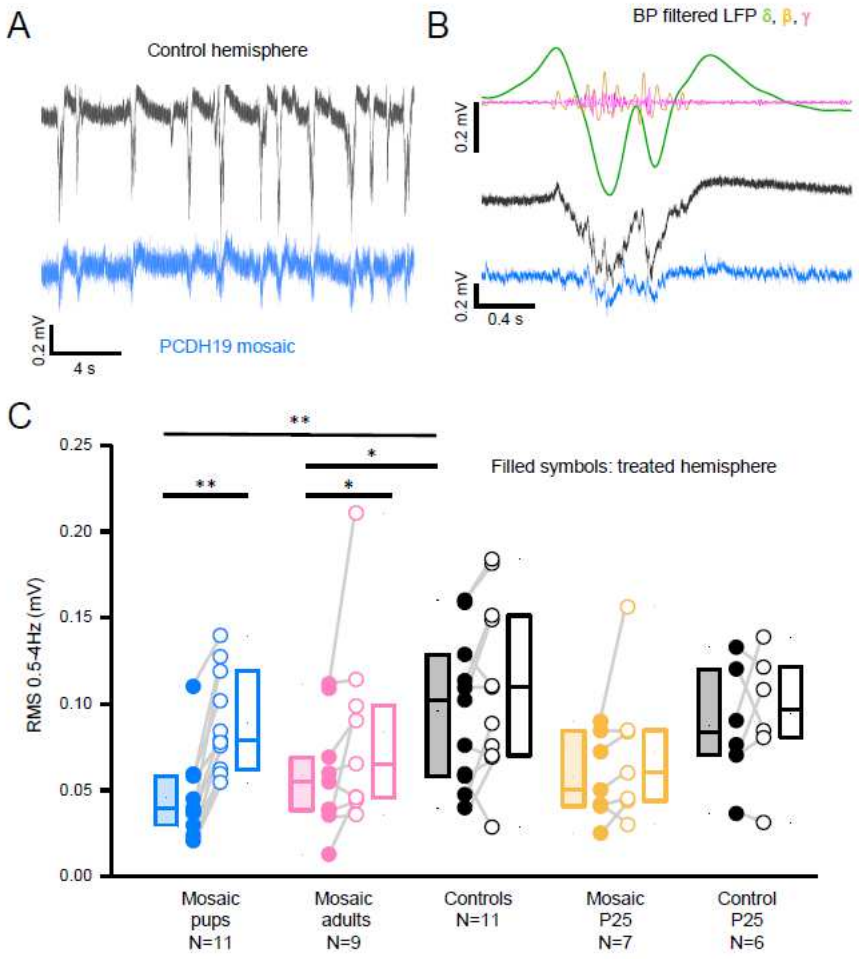

Figure 4. SWA is disrupted in PCDH19 mosaic patches. *A) Example LFP of a mosaic pup with reduced US amplitude in the injected hemisphere (blue trace) compared to the control hemisphere (black). B) The traces on the right show a close up of an US, with the band pass filtered signal of the control hemisphere in the δ (0.5-4 Hz; green), β (9-25 Hz; yellow), and γ (40-100 Hz; magenta) bands. C) Box plot (median, first and third interquartile) of RMS power in the 0.5-4 Hz range of the LFP. Significant differences are indicated with asterisks (** P<0.005, * P<0.05; Wilcoxon signed-rank test for paired measurements; Mann Whitney test for non-paired data).*

SWA is disrupted in PCDH19 mosaic patches

Mosaic mice displayed a second electrophysiological phenotype: a disruption of SWA specifically in the mosaic hemisphere (figure 4A). Quantification of SWA, in terms of root mean square (RMS) of the LFP signal filtered in the δ (0.5-4 Hz) range, confirmed that the reduction was highly significant (figure 4B). All recorded mice had reduced δ band activity in the injected hemisphere compared to the control hemisphere (figure 4C). Male and female mosaic mice showed

a similar phenotype and therefore data were grouped together (table S1). Other metrics of SWA were also significantly reduced (figure S2).

Interestingly, mice injected as adults also exhibited reduced SWA (figure 4C, figure S2C). This is in line with our previous findings of a hyperexcitable phenotype when mosaic expression is induced after the plastic period. The phenotype of the mice recorded in adolescence at P25 appeared to be milder since the reduced signal strength in the δ band was not significant (figure 4C).

Next, we aimed to understand why SWA is reduced in PCDH19 mosaic tissue. A reduction of synaptic strength and overall connectivity of the network underlies the decrement in slow wave strength occurring naturally over the course of sleep[23,24]. Such a reduction in functional connectivity was found to be associated with a reduction in the slope of USs, as the rate of recruitment and de-recruitment of neurons to and from the US decreases. To test whether a reduced connectivity might also underlie the SWA reduction in PCDH19 mosaic mice, we calculated the US slope (figure 5A,[24]). In all experimental groups, slopes were significantly reduced. Figure 5 depicts the maximum slope of the second segment of up states, but results were similar for the maximum slope of the first segment and for the average slopes (table S2). The differences were large in every mouse injected at P1 and were significant also in mice injected in adulthood (figure 5B). Strikingly, the mice recorded at adolescence hardly presented a phenotype (figure 5B) just as they did not for the reduction in SWA. This suggests that the reduction of SWA and of US slope are tightly coupled, as previously reported [23,24].

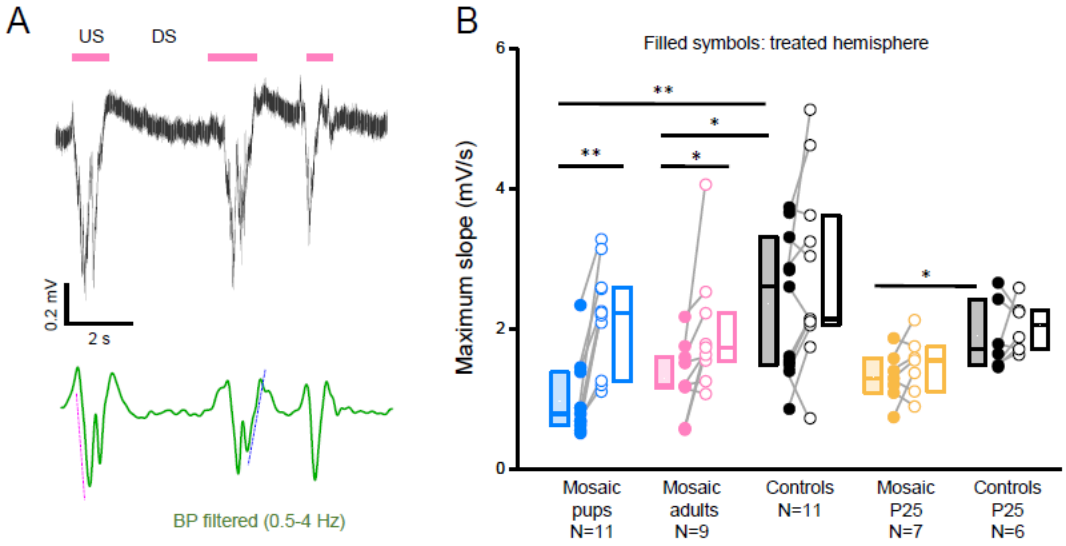

Figure 5: Reduction in SWA is associated with a reduced slope of state transitions*. A) Calculation of the US slope. Beginning and end of each US were identified from the LFP trace (black trace; magenta bars indicate USs). The signal was filtered in the δ band (0.5-4 Hz, green) and we computed the slope of both transitions from DS to US (magenta dashed line) and from US to DS (blue dashed line, see Materials & Methods). B) Box plots (median, first and third interquartile) of the slope of the transition from US to DS. Significant differences are indicated with asterisks (** P<0.005, * P<0.05; Wilcoxon signed-rank test for paired measurements; Mann Whitney test for non-paired data).*

Reduction in SWA is associated with reduced US slope and network synchronization

The finding that US slopes are reduced in PCDH19 mosaic mice, suggests that the network is less tightly coupled during SWA. Such a reduction in synaptic strength might lead to lower neuronal activity and firing. With this in mind, we extracted unit activity from our LFP recordings (figure 6A). We found a significant reduction in unit frequency in mice recorded in adulthood after being injected immediately after birth (Mosaic pups) or at P30 (Mosaic adults, figure 6B). Interestingly, we

also found that the percentage of units occurring within USs was significantly reduced in these mice (figure 6C). This demonstrates a lower synchronization of the network to the δ cycle, suggesting a lower degree of functional connectivity in the adult PCDH19 mosaics during deep sleep. Note however how units recorded in mice that displayed frequent β-oscillations were better synchronized to USs compared to other mosaic animals (black filled dots in figure 6C).

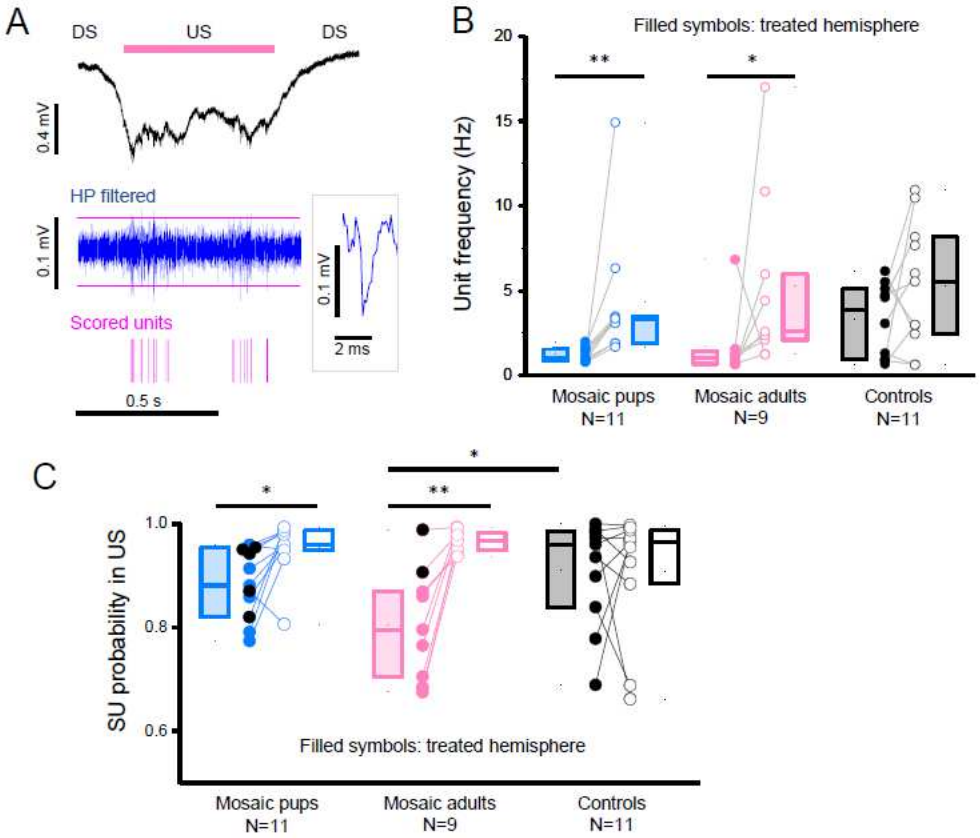

Figure 6. Unit activity is reduced and less synchronized in PCDH19 mosaic tissue. *A) Example of a LFP recording of a transition to an US (black trace) and corresponding high pass filtered trace (>300 Hz, blue) of a control animal recorded at P60. The magenta lines indicate the automatically calculated threshold, and the scored units are shown in the lower raster plot in magenta. Note how units cluster in the USs. The inset shows the magnification of a high passed unit. B,C) Box plots (median, first and third interquartile) of unit frequency (B) and of the probability of units (SU) to occur during Up states (C). In panel C, the black symbols represent mice with a hyperexcitable phenotype, defined as more than 5 ϐ bursts per hour. Significant differences are indicated with asterisks (** P<0.005, * P<0.05; Wilcoxon signed-rank test for paired measurements; Mann Whitney test for non-paired data).*

PCDH19 mosaic animals have an increased excitation to inhibition ratio

Finally, since both epilepsies and ASD's have been associated with a relative increase of excitation to inhibition[25,26], we investigated excitation to inhibition (E:I) ratio in PCDH19 mosaic mice. Recent work has demonstrated a strong correlation between E:I ratio and slope of the power spectrum of LFP and EEG recordings below 50 Hz[27], with a steeper slope resulting from relatively more inhibition. Therefore, we proceeded to calculate the power spectrum slope in our mice (figure S3).

PCDH19 mosaic animals displayed a significant reduction in the exponent of the fit exponential function (figure 7, table S3). The differences were also significant for mice recorded at

P25 but not for mice injected in adulthood. This suggests a slight increase in E:I ratio in our mice that is already present in adolescence. Indeed, when we applied γ-aminobutyric acid (GABA) to our P25 mice at the end of the experiment, the exponent dramatically increased in each recorded animal (figure 7, inset; and figure S3A). This implies that, as expected, increasing tonic inhibition by GABA application reduces the E:I ratio. Interestingly, GABA application also increased SWA in terms of the RMS signal strength in the 0.5-4 Hz range (figure S3B; see also the example LFP trace in figure S3A, right panel).

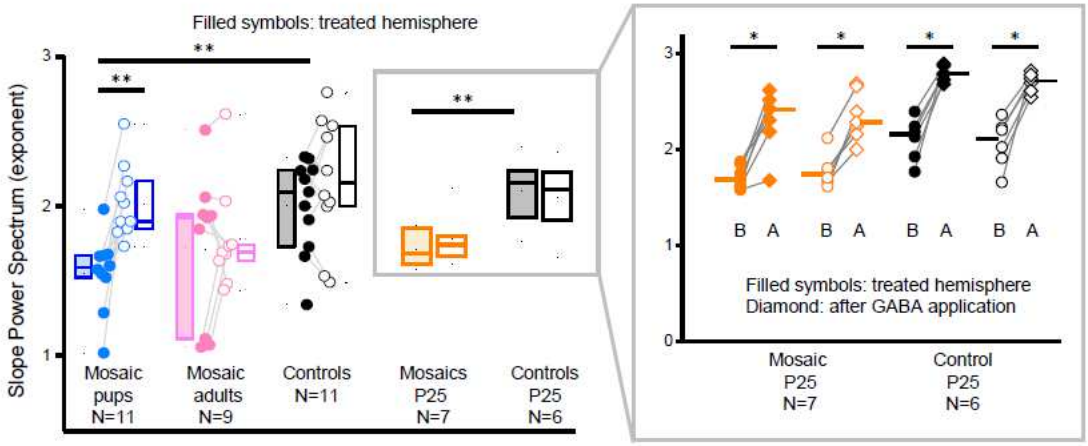

Figure 7. PCDH19 mosaic animals have an increased excitation to inhibition ratio. *Box plots of the slope of the LFP power spectrum (median, first and third interquartile). Significant differences are indicated with asterisks (** P<0.005, * P<0.05; Wilcoxon signed-rank test for paired measurements; Mann Whitney test for non-paired data). Power spectrum slopes were significantly reduced in 'Mosaic pups' and in animals recorded at P25. The inset contains the values of the same P25 mice shown in the main graph (boxed area) at the same scale and shows the values after ectopic application of GABA (B: before GABA; A: after GABA). Bars show median values, dots the average value per animal with lines connecting the value of each animal before and after GABA application. GABA significantly increases the slope in all cases.*

In vivo 2-photon calcium imaging in PCDH19 mosaic brain

We employed *in vivo* 2-photon calcium imaging to quantify activity of single neurons. As in the previous experiments, mice were injected with an AAV carrying EGFP-Cre recombinase directly after birth and recorded under urethane anaesthesia around P60. Two weeks prior to the experiment, mice were injected with an AAV expressing the red fluorescent calcium indicator jRGECO1a[28]. A representative field of view is shown in figure 8A, with 'red neurons' (wild-type; expressing only jRGECO1a) and 'green neurons' (knockout; expressing jRGECO1a as well as nuclear EGFP-Cre recombinase). We imaged calcium transients and recorded the LFP in the same hemisphere to evaluate the synchronization of calcium transients to USs. In control mice, the fluorescence fluctuations averaged on the entire field of view were closely phase locked to SWA (figure 8B). Individual neurons displayed transients more rarely than the US transitions (figure 8C), since firing occurs only sparsely with a majority of neurons being silent or producing only one action potential during each US[29].The rarity of the transients observed in controls (median frequency under 0.02 Hz, figure 8C) suggests that, in our imaging conditions we can only detect calcium transient when an individual neuron responds to an US with multiple spikes. Therefore, transient detection is intrinsically biased toward the population of more active cells. The distribution of transient frequencies has a larger dispersion in PCDH19 mosaics compared to controls (figure 8C; variance Bartlett's test: $P < 0.0001$). Interestingly, a similar increased variability of neuronal activity has been observed in a mouse model of Alzheimer's Disease[30]. There, the large variability was accompanied

by an increase in hyperactive neurons (neurons with > 4 calcium transients per minute). This population of hyperactive neurons was speculated to trigger seizures associated with Alzheimer's Disease and possibly a similar phenomenon might be taking place in PCDH19 mosaic mice. Indeed, in PCDH19 mosaic mice 26.1% of neurons were hyperactive, while only 7.8% of cells were hyperactive in the control (dotted line in figure 8C). The hyperactive neurons might underlie the observed hyperactive bursts in the mosaic tissue.

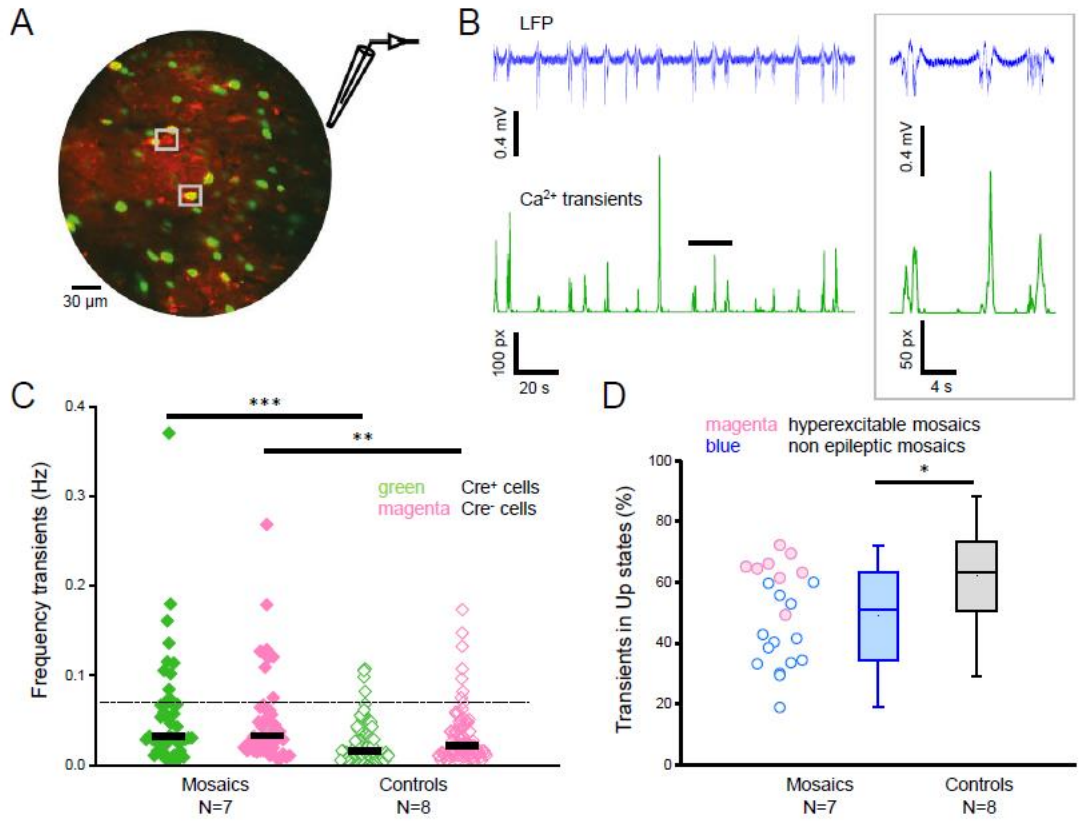

Figure 8. In vivo 2-photon calcium imaging in PCDH19 mosaic brain**. **A)** Example field of view with Cre-negative red neurons (top grey square; expressing jRGECO1a only) and Cre positive (PCDH19 knockout) green neurons (bottom square) that express jRGECO1a in the cytoplasm and EGFP-Cre recombinase in the nucleus. **B)** Calcium transients (green trace) measured on the entire field of view. The vertical axis displays the number of pixels affected by calcium activity over time (see Materials & Methods). The black trace shows the LFP recorded from the same hemisphere with an electrode positioned just outside of the imaged field at a depth of 250 µm. The inset shows magnified traces in correspondence of the black bar. Notice how Ca^{2+} transients are phase locked to the USs. **C)** Frequency of calcium transients in red and green cells of mosaic mice and controls. Each dot represents the average value for each active neuron. Significant differences are indicated with asterisks (P<0.0005, ** P<0.005; Mann Whitney test). Transient frequency is significantly increased in mosaics compared to control mice both for Cre^{+} (PCDH19 KO) neurons and for Cre^{-} neurons. **D)** Box plots of the percentage of Ca^{2+} transients occurring within USs, demonstrating a significant reduction in synchronisation to the SWA oscillation in mosaic mice compared to control mice (P=0.02; Mann Whitney test, whiskers indicate data range). Each dot represents the value obtained by all neurons in the imaging field of PCDH19 mosaic mice. The filled magenta dots, represent the values obtained from mosaic animals with a hyperexcitable (>5 β oscillations per hour) phenotype, the blue dots from all other mosaics.*

Finally, calcium transients in mosaic animals were less synchronized to SWA than in controls, as shown by a reduction in the percentage of transients occurring during USs (figure 8D). This agrees with the SU analysis (figure 6). Interestingly, mosaic animals with a hyperexcitable phenotype (>5 β-

oscillations per hour) seemed to have a higher degree of synchronization to SWA than non-epileptic mosaics (figure 8D; red versus blue dots). This difference is statistically significant ($P<0.0005$) and it confirms the results from our LFP recordings: PCDH19 mosaic mice that display epileptic-like activity have a larger degree of synchronicity to SWA than non-epileptic mosaic mice (figure 6C).

Discussion

Pcdh19 is becoming one of the most clinically relevant genes in epilepsy, yet little is known about its function. Here, we performed a thorough electrophysiological characterization of cortical activity in a novel mouse model of the disease and found that a mosaic network not only displays signs of hyperexcitability, but also severe disruptions of SWA, a crucial component of NREM sleep. Additional analyses suggested an increased E:I ratio and reduced coupling of the network. Furthermore, we have shown that PCDH19 is required also during adult life, as its loss in early adulthood caused the onset of the disease. Finally, calcium imaging experiments implied that the hyperexcitable phenotype might derive from a population of hyperactive neurons present in the mosaic network.

Hyperactivity and hyperexcitability of the PCDH19 mosaic patch

Given the cortical dysplasia and folding abnormalities in some patients[11,31–33] and the large patches of PCDH19 expression in mouse models[11,12], it is likely that the mosaic is not only represented by a random mix of neurons with the two genotypes, but also by mosaicism on a large scale with patches of reduced PCDH19 expression interspersed in brain tissue with normal PCDH19 expression. This condition would be recapitulated by our model: indeed, even if PCDH19 mosaicism occurs only in a relatively small portion of the cortex, we observed a hyperactive behavioural phenotype, consistent with the clinical features of the disease[34].

Hyperactivity and epilepsy are frequent co-morbidities[34,35] and, indeed, we observed two signs of hyperexcitability in our mouse model: oscillations in the β (9-25 Hz) band and large amplitude 'hypersynchronous' peaks. We never recorded true ictal events, which given the short duration of our recordings (2-4 hours) is not surprising. The phenotype we observed in adult mice is relatively mild consistently with the observation that in patients epilepsy fades in severity in adulthood[6,36]. Interestingly, the mortality peak of our mosaic mice was around adolescence and at these time mice exhibited a more severe electrophysiological phenotype.

Our data show a clear relationship between SWA and epileptiform activity: hypersynchronous peaks tended to occur during USs and β-oscillations, recorded in the EEGs, occurred mainly during NREM sleep. Indeed, it is known that seizures[37] and interictal spikes[38] are more likely to occur during slow wave sleep than during REM sleep or wake and that they are associated with slow waves[39,40]. In fact, in PCDH19 patients, seizures occur primarily during sleep[41]. Altogether, these data confirm that the mouse model recapitulates important features of patients and that it provides a model to study how hyperexcitable activity arises in PCDH19 mosaic tissue and how it can be mitigated by pharmacological treatments.

Development of the phenotype

In patients, the phenotype changes in adolescence, when seizures tend to decrease in frequency and the behavioural features become the most prominent aspect of the disease[4,6]. This developmental switch is also present in our data, since epileptiform bursts are more frequent in adolescents (P25) than in adults (P60), while the disruption of SWA observed in adults is hardly present in adolescent mice. We could speculate that the reduced synaptic strength and synchronicity during SWA could represent a compensatory mechanism to prevent hypersynchronous

activity triggered by the transitions to USs. This scenario is compatible with the observation that mice displaying the highest degree of synchronization to SWA were also characterized by frequent β-oscillations.

In addition, it is conceivable that, the progressive loss of SWA in mosaic mice reflects a different function of PCDH19 in the developing network versus a mature network. Our data support the idea that PCDH19 plays a role in synapse and circuit maintenance throughout life, since mice injected with Cre-AAV as adults displayed a phenotype, both in terms of hyperexcitability and SWA disruption. This data is consistent with the recent finding that reduced expression of the clock gene BMAL1 in adult mice causes a loss of PCDH19 expression and an increase in susceptibility to epilepsy[42]. These findings have important implications for patients as it means that at least some of the symptoms are caused by the role of PCDH19 in the mature brain and could possibly be reversed by correcting gene function later in life.

SWA disruptions and possible implications on cognitive deficits

SWA has been shown to aid in memory consolidation during sleep[43,44] and to be important for cognitive functions. On a network level, SWA has been hypothesized to restore overall synaptic strength of the network[45] by operating synaptic downscaling[46–48]. Interestingly, while high-firing neurons reduce their activity during NREM sleep, neurons that fire at a low rate increase theirs. In this manner, sleep homogenizes the firing rate distribution[49]. We observed a large variability of neuronal activity in PCDH19 mosaic tissue. This might be partly caused by the lack of slow wave sleep's homogenizing effect on firing rates leading to an unstable network in PCDH19 mosaic. Disruptions of SWA in PCDH19 patients would therefore likely affect their cognitive performance and might partly underlie the intellectual disability frequently associated with the disease.

Growing evidence suggest that sleep is affected in PCDH19 patients as they frequently experience difficulties in falling and staying asleep[50]. Recently, a polysomnography study on a PCDH19 patient complaining of prolonged nocturnal awakenings, revealed abnormal NREM sleep episodes. Normal slow waves co-occurred with rapid eye movements typical of REM sleep, a rare state dissociation where NREM sleep appears to be intruded by REM sleep[51]. Our behavioural assessment of sleep and the electrophysiological assessment of SWA suggest that sleep disturbances are an important component of the PCDH19 phenotype also in the mouse model.

Network activity in PCDH19 mosaic tissue

The analysis of network activity of PCDH19 mosaic tissue has shown an increased E:I ratio as well as reductions in SWA, up state slope, and synchronicity of neuronal firing to SWA. Many of the observed effects are common features of ASD's, epilepsies, and schizophrenia[25,52,53]. Interestingly, schizophrenia is a late-onset feature of PCDH19 Epilepsy[52]. A proper E:I ratio is crucial for network computation[25]. Elevating the E:I ratio in mice has been demonstrated to impair neuronal information processing by saturating their input-output curve[53]. Additionally, a proper E:I balance is needed to maintain stable firing rates in a feedforward neural network[54].

The finding that the PCDH19 network is characterized by reduced synaptic coupling appears to be at odds with a hyperexcitable phenotype. This apparent contradiction has been observed elsewhere: for example, in Rett syndrome firing rates appear to be reduced[55]. Additionally, increased inhibitory activity has been linked to epileptiform activity[56,57]. Indeed, the relationship between synaptic strength and firing rates is not clear-cut. Reductions in synaptic coupling do not necessarily reduce firing rates nor does an increased E:I ratio inevitably increase firing rates[27]. In fact, many ASD mouse models show no changes or even reductions in pyramidal firing rates despite reduced inhibition and susceptibility to seizures[26]. It is conceivable that network homeostasis resulting from an increased E:I ratio cannot maintain stable firing rates[26,58]. Such a network would display a large variability in activity, as is the case in PCDH19 mosaic mice, and consequently be unstable. Some examples in literature suggest a link between epileptic-like activity and increased variability of

activity accompanied by a population of hyperactive neurons. One of these examples is Alzheimer's Disease[30,59], where the population of hyperactive neurons not only displays a high firing rate but also highly correlated firing, increasing the risk for seizure-like activity[30].

Conclusions

We present an extensive electrophysiological characterization of cortical activity in a mouse model of PCDH19 Epilepsy. These mice display behavioural hyperactivity, signs of hyperexcitability, and disrupted SWA. We additionally found that PCDH19 Epilepsy is not merely a neurodevelopmental disease and that some of the symptoms might arise from disturbed PCDH19 function in the mature network. Finally, our data suggest that the PCDH19 mosaic network is less strongly coupled, less synchronized, displays increases in E:I ratio, and has a large variability of neuronal activity with a population of hyperactive neurons. We propose that the behavioural and cognitive problems derive from a reduced network coupling, while the bursting of hyperactive neurons underlies the hyperexcitable phenotype.

Contributions

The study was designed by DL and GMR. The floxed PDH19 mouse was designed by SB, MPass and SMa. The in-situ hybridizations were performed by MPasq and SMi. Actogram experiments were performed by GMR and FC. All in vivo recordings from anesthetized mice were performed by DL with contributions from SL, RM and VP. The recordings from behaving mice were performed by LB, DL and SL. Two photon Ca imaging was performed by DL. Data analysis and curation: DL. Custom code for this project was written by DL, GMR and FC. The manuscript was written by DL and GMR with contributions by SL and all other authors. The study was supported by Telethon (grant GP19281 to GMR) and by Regione Toscana (grant DECODE-EE to GMR).

References

1. Duszyc, K., Terczynska, I. & Hoffman-Zacharska, D. Epilepsy and mental retardation restricted to females: X-linked epileptic infantile encephalopathy of unusual inheritance. *Journal of Applied Genetics* **56**, 49–56 (2015).
2. Scheffer, I. E. *et al.* Epilepsy and mental retardation limited to females: an under-recognized disorder. *Brain* **131**, 918–927 (2008).
3. Depienne, C. *et al.* Sporadic infantile epileptic encephalopathy caused by mutations in PCDH19 resembles dravet syndrome but mainly affects females. *PLoS Genet.* **5**, e1000381 (2009).
4. Kolc, K. L. *et al.* A systematic review and meta-analysis of 271 PCDH19-variant individuals identifies psychiatric comorbidities, and association of seizure onset and disease severity. *Molecular Psychiatry* (2018). doi:10.1038/s41380-018-0066-9
5. Vlaskamp, D. R. M. *et al.* Schizophrenia is a later-onset feature of PCDH19 Girls Clustering Epilepsy. *Epilepsia* **60**, 429–440 (2019).
6. Depienne, C. *et al.* Mutations and deletions in PCDH19 account for various familial or isolated epilepsies in females. *Hum. Mutat.* **32**, 1959–1975 (2011).
7. Specchio, N. *et al.* Spectrum of phenotypes in female patients with epilepsy due to protocadherin 19 mutations. *Epilepsia* **52**, 1251–1257 (2011).
8. Dibbens, L. M. *et al.* X-linked protocadherin 19 mutations cause female-limited epilepsy and cognitive impairment. *Nat. Genet.* **40**, 776–781 (2008).
9. Thiffault, I. *et al.* PCDH19-related epileptic encephalopathy in a male mosaic for a truncating variant. *Am. J. Med. Genet. Part A* **170**, (2016).
10. de Lange, I. M. *et al.* Male patients affected by mosaic PCDH19 mutations: five new cases. *Neurogenetics* **18**, 147–153 (2017).
11. Pederick, D. T. *et al.* Abnormal Cell Sorting Underlies the Unique X-Linked Inheritance of PCDH19 Epilepsy. *Neuron* **97**, 59–66 (2018).
12. Hayashi, S. *et al.* Loss of X-linked Protocadherin-19 differentially affects the behavior of heterozygous female and hemizygous male mice. *Sci. Rep.* **7**, (2017).
13. Hoshina, N., Johnson-Venkatesh, E. M., Hoshina, M. & Umemori, H. Female-specific synaptic dysfunction and cognitive impairment in a mouse model of PCDH19 disorder. *Science* **372**, (2021).
14. Bassani, S. *et al.* The female epilepsy protein PCDH19 is a new GABAAR-binding partner that regulates GABAergic transmission as well as migration and morphological maturation of hippocampal neurons. *Hum. Mol. Genet.* **27**, 1027–1038 (2018).
15. Serratto, G. M. *et al.* The Epilepsy-Related Protein PCDH19 Regulates Tonic Inhibition, GABAAR Kinetics, and the Intrinsic Excitability of Hippocampal Neurons. *Mol. Neurobiol.* (2020). doi:10.1007/s12035-020-02099-7
16. Brust, V., Schindler, P. M. & Lewejohann, L. Lifetime development of behavioural phenotype in the house mouse (Mus musculus). *Front. Zool.* **12**, (2015).
17. Steriade, M., Nuñez, A. & Amzica, F. A novel slow ({\textless} 1 Hz) oscillation of neocortical neurons in vivo: depolarizing and hyperpolarizing components. *J. Neurosci.* **13**, 3252–3265 (1993).
18. Neske, G. T. The Slow Oscillation in Cortical and Thalamic Networks: Mechanisms and Functions. *Front. Neural Circuits* **9**, (2016).
19. Trovato, F. *et al.* A Cre-amplifier to generate and detect genetic mosaics in vivo. *bioRxiv Prepr.* 1–21 (2019). doi:10.1101/715490
20. De Curtis, M. & Avanzini, G. Interictal spikes in focal epileptogenesis. *Prog. Neurobiol.* **63**, 541–567 (2001).
21. Fisher, R. S. *et al.* Epileptic Seizures and Epilepsy: Definitions proposed by the International

League Against Epilepsy (ILAE) and the International Bureau for Epilepsy (IBE). *Epilepsia* **46**, 470–472 (2005).
22. Petrucco, L., Pracucci, E., Brondi, M., Ratto, G. M. & Landi, S. Epileptiform activity in the mouse visual cortex interferes with cortical processing in connected areas. *Sci. Rep.* **7**, (2017).
23. Esser, S. K., Hill, S. L. & Tononi, G. Sleep Homeostasis and Cortical Synchronization: I. Modeling the Effects of Synaptic Strength on Sleep Slow Waves. *Sleep* **30**, 1617–1630 (2007).
24. Vyazovskiy, V. V, Riedner, B. A., Cirelli, C. & Tononi, G. Sleep homeostasis and cortical synchronization: II. A local field potential study of sleep slow waves in the rat. *Sleep* **30**, 1631–1642 (2007).
25. Rubenstein, J. L. R. & Merzenich, M. M. Model of autism: increased ratio of excitation/inhibition in key neural systems. *Genes, Brain Behav.* **2**, 255–267 (2003).
26. Antoine, M. W., Langberg, T., Schnepel, P. & Feldman, D. E. Increased Excitation-Inhibition Ratio Stabilizes Synapse and Circuit Excitability in Four Autism Mouse Models. *Neuron* **101**, 648–661 (2019).
27. Gao, R., Peterson, E. J. & Voytek, B. Inferring synaptic excitation/inhibition balance from field potentials. *Neuroimage* **158**, 70–78 (2017).
28. Dana, H. *et al.* Sensitive red protein calcium indicators for imaging neural activity. *Elife* **5**, (2016).
29. Neske, G. T., Patrick, S. L. & Connors, B. W. Contributions of diverse excitatory and inhibitory neurons to recurrent network activity in cerebral cortex. *J. Neurosci.* **35**, 1089–1105 (2015).
30. Busche, M. A. *et al.* Clusters of Hyperactive Neurons Near Amyloid Plaques in a Mouse Model of Alzheimer's Disease. *Science (80-.).* **321**, 1686–1690 (2008).
31. Ryan, S. G. *et al.* Epilepsy and mental retardation limited to females: an X-linked dominant disorder with male sparing. *Nat. Genet.* **17**, 92–95 (1997).
32. Kurian, M. *et al.* Focal cortical malformations in children with early infantile epilepsy and PCDH19 mutations: case report. *Dev. Med. Child Neurol.* **60**, (2018).
33. Lenge, M. *et al.* Quantitative MRI-Based Analysis Identifies Developmental Limbic Abnormalities in PCDH19 Encephalopathy. *Cereb. Cortex* **00**, 1–12 (2020).
34. Kolc, K. L. *et al.* PCDH19 Pathogenic Variants in Males : Expanding the Phenotypic Spectrum. *Adv. Exp. Med. Biol.* (2020).
35. Parisi, P., Moavero, R., Verrotti, A. & Curatolo, P. Attention deficit hyperactivity disorder in children with epilepsy. *Brain Dev.* **32**, 10–16 (2010).
36. Kolc, K. L. *et al.* A systematic review and meta-analysis of 271 PCDH19-variant individuals identifies psychiatric comorbidities, and association of seizure onset and disease severity. *Mol. Psychiatry* **24**, 241–251 (2019).
37. Terzano, M. G., Parrino, L., Garofalo, P. G., Durisotti, C. & Filati-roso, C. Activation of partial seizures with motor signs during cyclic alternating pattern in human sleep. *Epilepsy Res.* **10**, 166–173 (1991).
38. Sammaritano, M., Gigli, G. L. & Gotman, J. Interictal spiking during wakefulness and sleep and the localization of foci in temporal lobe epilepsy. *Neurology* **41**, 290–297 (1991).
39. De Guzman, P. H., Nazer, F. & Dickson, C. T. Short-duration epileptic discharges show a distinct phase preference during ongoing hippocampal slow oscillations. *J. Neurophysiol.* **104**, 2194–2202 (2010).
40. Frauscher, B. *et al.* Facilitation of epileptic activity during sleep is mediated by high amplitude slow waves. *Brain* **138**, 1629–1641 (2015).
41. Ikeda, H. *et al.* Characteristic phasic evolution of convulsive seizure in PCDH19-related epilepsy. *Epileptic Disord.* **18**, 26–33 (2016).
42. Wu, H. *et al.* Decreased expression of the clock gene Bmal1 is involved in the pathogenesis of temporal lobe epilepsy. *Mol. Brain* **14**, 113 (2021).
43. Marshall, L. & Born, J. The contribution of sleep to hippocampus-dependent memory consolidation. *Trends Cogn. Sci.* **11**, 442–450 (2007).

44. Rasch, B. & Born, J. About sleep's role in memory. *Physiol. Rev.* **93**, 681–766 (2013).
45. Tononi, G. & Cirelli, C. Sleep and the Price of Plasticity: From Synaptic to cellular Homeostasis to Memory Consolidation and Integration. *Neuron* **81**, 12–34 (2014).
46. Vyazovskiy, V. V, Cirelli, C., Pfister-genskow, M., Faraguna, U. & Tononi, G. Molecular and electrophysiological evidence for net synaptic potentiation in wake and depression in sleep. *Nat. Neurosci.* **11**, 200–208 (2008).
47. Vyazovskiy, V. V *et al.* Cortical firing and sleep homeostasis. *Neuron* **63**, 865–878 (2009).
48. de Vivo, L. *et al.* Ultrastructural Evidence for Synaptic Scaling Across the Wake/Sleep Cycle. *Science (80-.).* **355**, 507–510 (2017).
49. Watson, B. O., Levenstein, D., Greene, J. P., Gelinas, J. N. & Buzsaki, G. Network Homeostasis and State Dynamics of Neocortical Sleep. *Neuron* **90**, 839–852 (2016).
50. Smith, L. *et al.* PCDH19-related epilepsy is associated with a broad neurodevelopmental spectrum. *Epilepsia* **59**, 679–689 (2018).
51. Rupin-Mas, M., Gourfinkel-An, I. & Arnulf, I. N3 sleep with rapid eye movements in a PCDH19 mutation: a new dissociate state between N3 and REM sleep. *Sleep Med.* **74**, 341–342 (2020).
52. Bozzi, Y., Provenzano, G. & Casarosa, S. Neurobiological bases of autism–epilepsy comorbidity: a focus on excitation/inhibition imbalance. *Eur. J. Neurosci.* **47**, 534–548 (2018).
53. Yizhar, O. *et al.* Neocortical excitation/inhibition balance in information processing and social dysfunction. *Nature* **477**, 171–178 (2011).
54. Zhou, S. & Yu, Y. Synaptic E-I balance underlies efficient neural coding. *Front. Neurosci.* **12**, (2018).
55. Dani, V. S. *et al.* Reduced cortical activity due to a shift in the balance between excitation and inhibition in a mouse model of Rett Syndrome. *Proc. Natl. Acad. Sci.* **102**, 12560–12565 (2005).
56. Gnatkovsky, V., Librizzi, L., Trombin, F. & De Curtis, M. Fast activity at seizure onset is mediated by inhibitory circuits in the entorhinal cortex in vitro. *Ann. Neurol.* **64**, 674–686 (2008).
57. Avoli, M. & de Curtis, M. GABAergic synchronization in the limbic system and its role in the generation of epileptiform activity. *Prog. Neurobiol.* **95**, 104–132 (2011).
58. Goel, A. & Portera-Cailliau, C. Autism in the Balance: Elevated E-I Ratio as a Homeostatic Stabilization of Synaptic Drive. *Neuron* **101**, 543–545 (2019).
59. Kastanenka, K. V *et al.* Optogenetic restoration of disrupted slow oscillations halts amyloid deposition and restores calcium homeostasis in an animal model of Alzheimer's disease. *PLoS One* **12**, 1–25 (2017).

Materials and Methods

Animals and Genotyping

A 727 bp long region surrounding exon 3 of PCDH19 was flanked by LoxP sites in mice with a C57BL/6 background (mixed J and N). Mice were housed in a 12 hr light:dark cycle (light on at 7 AM and light off at 7 PM) with ad libitum access to food and water. Mice were genotyped by separation of PCR products (F primer 5'-TCTCCCCCATAGGCTCAACTTTCC- 3' and R primer 5'-AGTGCCTTTAGGATTCCGAACCACAGG-3') using agarose gel electrophoresis (yielding a wild-type band of 1053 bp and a floxed one of 1224 bp). All experiments were performed during the day (between 8:30 AM and 6:00 PM). Both males and females were used in this study and - since they showed similar activity in the LFP recordings (*Supplementary table 1*) - their data were pooled. All procedures were approved by the Italian Ministry of Health (Permit number 465-2018-PR).

We included three experimental groups in our measurements: a group of mice consisting of 4 males and 7 females injected directly after birth (at postnatal day 1; P1) and measured in adulthood (around P60), a second group injected at P1 and measured in puberty (around P25), and a third group injected as adults (older than P60) and measured at least 30 days later.

Viral injections

Mosaic PCDH19 expression was induced in the occipital cortex of PCDH19 conditional knockout mice by focal injection of an AAV expressing EGFP-Cre recombinase (Addgene #105545-AAV1; pAAV.CMV.HI.eGFP-Cre.WPRE.SV40). Control mice were either non-floxed littermates injected with EGFP-Cre recombinase or floxed littermates injected with an AAV expressing EGFP (Addgene #105530-AAV5; pAAV.CMV.PI.EGFP.WPRE.bGH). The control groups showed similar results and were therefore pooled. Mice were injected either directly after birth (P1-3) or as adults for the experimental group 'Mosaic adults' (>P60). Mice employed in the Ca^{2+} imaging experiments were injected twice: they received the Cre recombinase AAV vector at P1 and a second injection at about P40 with a genetically encoded calcium sensor (Addgene #100854-AAV1; pAAV.Syn.NES-jRGECO1a.WPRE.SV40).

The procedure was similar for pups and adults. Pups were anesthetized with isoflurane (Iso-Vet; 5% during induction, 1.5% during the surgery; 200 mL air) delivered through a mouth mask, and adults with a peritoneal injection of avertin (0.2 mL per 10 gr mouse). Anaesthesia level was assessed using a tail pinch. Mice were fixed in a stereotactic frame and a small incision was made in the skin. The skull was cleaned with 70% ethanol and then pierced at the target site using a needle in pups or a surgical drill in adults. We targeted an area slightly medial to V1 (2.7 mm posterior to bregma and 2.4 mm lateral to lambda) in the right hemisphere of the mice to prevent causing damage to the recording site. A small glass capillary (40 µm diameter) was slowly lowered into the brain to a depth of 350 µm in pups and 400 µm in adults. Roughly 0.7 µL of virus was injected at a rate of 100 nL/min. After removal of the capillary from the brain, the skull was cleaned again with 70% ethanol and for adults the skin was sutured with a non-absorbable 3-0 filament (Ethicon). Finally, an antiseptic (Betadine) was applied on the skin and the mouse was kept in a warm environment till full recovery.

In vivo local field potential recordings

Animals were prepared for *in vivo* LFP recordings as described previously (Petrucco et al., 2017; Trovato et al., 2020). Mice were injected intraperitoneally with urethane (dissolved in 0.9% NaCl; 0.08 mL per 10 gr mouse). Throughout the procedure, the state of the animal was regularly assessed, and an additional dose of urethane was administered if needed (10% of the initial dose). Recordings lasted around 2-4 hrs and at the end of the experiment deeply anesthetized mice were sacrificed by cervical dislocation without regaining consciousness.

The head was fixed in a stereotactic frame, the skin opened and the skull cleaned. A 2-3 mm craniotomy was drilled over the occipital cortex (2.7 mm posterior to bregma and 2.5 mm lateral to lamba) in both hemispheres with the dura mater left intact. A bath containing ACSF was created by surrounding the craniotomy with a thin layer of dental cement. In this way, the cortex could be kept constantly wet. A common reference Ag-AgCl electrode was placed in the bath, while LFPs were recorded with glass micropipettes (impedance ~ 2 MΩ; filled with ACSF) placed at a depth of 250-300 µm to record from cortical layers II/III using a motorized micromanipulator (Sutter Instrument MPC-200). In the case of γ-aminobutyric acid (GABA; Sigma Aldrich) application, the drug was dissolved in ACSF to a concentration of 5 mM. We then replaced the ACSF in the bath with the ACSF containing GABA, waited for 5 min, recorded for 7.5 min, waited another 5 min and then recorded again for 7.5 min.

LFP signals were amplified 1000 times (EXT-02F amplifiers; NPI electronic), band pass filtered (0.1-1000 Hz), cleared from 50 Hz interference (Hum Bug Noise Eliminator; Quest Scientific), and finally oversampled at 10 kHz with 16-bit precision (AD board USB6251; National Instruments).

EEG recordings in behaving mice

Mice were implanted with an EEG headmount (containing 2 EEG channels and 1 EMG; #8201; Pinnacle Technology Inc) one week prior to the recording. Mice were anesthetized with a peritoneal injection of isoflurane (1-4%), fixed in a stereotactic frame, and a cut was made in the skin on top of their skull. The skull was then thoroughly cleaned with a 70% ethanol solution and the headmount glued to the skull. The headmount was further fixed with stainless steel screws placed deep into the skull in contact with the brain surface. These screws served as electrodes and were placed in such a way that the 2 EEG channels were placed above the occipital cortex, 1 in each hemisphere, with their corresponding reference electrodes placed more frontally in the same hemisphere. EMG wires were placed in the trapezius muscles of the mice. The head-mount was further fixed with dental cement and the mice were kept in a warm spot until recovered from the anaesthesia.

Mice were habituated to the recording room for at least 24 hours before being recorded for at least 24 hours. To record the mice, a pre-amplifier (#8202-SL; Pinnacle Technology) providing 100 times amplification and high pass filtering of the EEG (0.5 Hz) and EMG (10 Hz) channels was connected to the headmount. The signals were routed to a data acquisition system (#8206, Pinnacle Technology Inc) which provided additional filtering (low pass at 100 Hz for the EEG channels and 200 Hz for the EMG channel). The data were sampled at 400 Hz, send to a PC and exported in edf format with Sirenia Software 1.7.9 (Pinnacle Technology Inc) for further analyses.

In vivo 2-photon calcium imaging

Mice prepared for the imaging experiments received only one craniotomy in the right hemisphere that was sealed with a perforated glass window. The LFP was recorded by a glass electrode inserted through the coverslip perforation at an angle of 25°. LFP traces were sampled at 2 kHz.

Imaging was performed with a 2-photon microscope (Ultima IV; Prairie Technologies) and 18 W Ti:Sapphire laser (Chameleon Ultra 2; Coherent) delivering 20-30 mW of light to the sample. Time series were acquired at 8.05 Hz (a period of 0.1241 s; 1500 repetitions) at a similar depth of the LFP recordings (200-300 µm) in spiral scan mode. A 20X water immersion objective was used (N20X-PFH-20X Olympus XLUMPLFLN Objective; 1.00 NA) at a resolution of 256*256 pixels and a zoom of 2, leading to an effective resolution of 1.2 µm per pixel and a field of view of about 305*305 µm. Two wavelengths were used: the presence of EGFP was assessed by excitation at 980 nm, while calcium activity was monitored by excitation of the jRGECO1a sensor at 1040 nm.

Molecular Biology and immunohistochemistry

Western Blots were performed on 3 control (injected with an AAV expressing EGFP) and 3 treated (injected with an AAV expressing EGFP-Cre recombinase) mice injected at P1. At the end of the LFP recording, anesthetized mice were sacrificed by cervical dislocation and a portion of the fluorescent area of the cortex, as well as a portion of cortex from the opposite non-injected hemisphere, was obtained from each mouse. Samples were flash frozen on dry ice and then transferred to -80 °C.

Samples underwent homogenization in modified Radio Immunoprecipitation Assay (RIPA) buffer (50 mM Tris – HCl, 150 mM NaCl, 1 mM EDTA, 1% NP – 40, 1% Triton X100, pH 7.4 and protease inhibitors) and then mixed with Sample Buffer 3X. Homogenates underwent SDS–PAGE and protein were transferred to a 0.2 µm nitrocellulose support (Amersham GE Healthcare) through a wet–tank system (Bio–Rad). Membranes were blocked in 5% skim milk in Tris Buffer Saline (TBS) for 1 hour at room temperature and then washed in TBS with 0,1% Tween 20 detergent (TBST) for 5 minutes at room temperature. Membranes were incubated with primary antibodies prepared in 5% skim milk in TBST 0,1% overnight at 4°C (PCDH19 1:20000, Bethyl Laboratories; GAPDH 1:2000, Santa Cruz Biotechnology). After washing (3 times for 10 min with TBST and twice for 15 min with TBS), membranes were incubated with secondary antibodies for 1 hour at room temperature (1:7500, Li-Cor). Proteins were detected by using the Odyssey CLx detector system and quantified by Image Studio software program.

Combined in situ hybridization (ISH) and immunohistochemistry (IHC) analysis for PCDH19 exon 1 and EGFP was performed on floxed (mosaic) and non-floxed (control) adult mice injected at P1 with EGFP-Cre recombinase as previously described (Napolitano et al, 2019; PMID: 31653935; DOI: 10.1038/s41598-019-51839-w). Briefly, deeply anesthetized mice were sacrificed at the end of the experiment and their brains quickly dissected, embedded in TissueTek (Sakura) and frozen at 80 °C. Fourteen-micrometre cryosections were cut on the coronal plane incubated overnight at 4 °C with primary mouse anti-EGFP antibody (1:2000, Thermo Fisher Scientific Inc.), followed by a 2-hour incubation at room temperature with an Alexa Fluor 488 goat anti-rabbit antibody (1:500, Thermo Fisher Scientific Inc.). Following IHC, ISH was performed using a fluorescein-labeled *Pcdh19* antisense riboprobe (0.9 Kb). A chromogenic reaction using NBT/BCIP substrate solution (Roche) was performed to visualize the dig-labelled riboprobe. Images were acquired with a Nikon SMZ18 (low magnification images; SHR plan apo 1x objective; Supplementary figure 1D left) and a Zeiss Airyscan (20x water immersion objective; Supplementary figure 1D right).

Immunohistochemistry for Cre recombinase was performed on the brains of most of the recorded animals injected at P1. At the end of the LFP recording, deeply anesthetized mice were transcardially perfused with 4% paraformaldehyde without regaining consciousness. Coronal brain sections (60 µm thick) were cut using a vibratome and rinsed 3 times for 15 min with PBS. Blocking was performed for 1 hr at room temperature (blocking solution: 3% BSA; 0.4% Triton-X100; in PBS). Sections were incubated with primary antibody in blocking solution (mouse anti-Cre; 1:100; Sigma Aldrich) overnight at 4 °C, rinsed 3 times in PBS, and incubated with secondary antibody (anti-mouse TRITC; 1:300; Sigma Aldrich) for 1 hr at room temperature. After 3 additional rinsing steps in PBS, slices were mounted in Fluoroshield™ with DAPI (Sigma Aldrich) to stain nuclei.

Data analyses: electrophysiology

The electrophysiological data were analyzed using a custom written software suite in MATLAB (The MathWorks Inc.). The code is available on Github (https://github.com/DidiLamers/PCDH19_ZebraExplore). LFP traces were band-pass filtered with zero phase distortion. Signal strength in various frequency bands was calculated by computing the root mean square (RMS) of the filtered signal. The frequency-time analysis was calculated by computing the RMS of the filtered signal in a moving 0.25 s window with 0.05 s overlap. Up states were detected by analysis of the distribution of the logarithm of signal strength in the β-σ (9-25 Hz) band over time. This distribution was bimodal, in correspondence with up states (high β signal

strength) and down states (low β signal strength). The distribution was fitted with two Gaussian curves, and the threshold was set at the intersection of the two distributions. The automated segmentation of the LFP data allowed the non-assisted computation of all metrics relative to SWA.

Up state slopes were calculated based on Esser et al., 2007 and Vyazovskiy et al., 2007. In brief, we computed the LFP filtered in the δ (0.5-4 Hz) range between the start and end time of each detected up state. The average slope was calculated by dividing the amplitude of the most prominent negative peak by the interval elapsing from either the previous zero crossing (first segment of the up state) or the subsequent zero crossing (second segment of the up state).

Units were extracted from the data as suggested by Quiroga et al., 2004. Briefly, we high-pass filtered the LFP at 300 Hz as described above. We then automatically set a threshold according to

$$Thr = 4 * median\left\{\frac{|x|}{0.6745}\right\}$$

where x is the filtered LFP. Spikes crossing the threshold were labelled as units and their frequency and correlation with up state timing was determined.

The slope of the power spectrum was computed according to an algorithm developed by Donoghue et al., 2020 (https://github.com/DidiLamers/PCDH19_FOOOF). First, we calculated the power spectrum of each LFP trace using a multitaper method (*mtspectrumc* function of the Chronux Toolbox; Bokil et al., 2010). These power spectra were then fitted with an aperiodic signal $(1/f)$ and periodic oscillatory components based on Gaussian model fits. The aperiodic exponential function

$$L = b - \log\left(k + F^X\right)$$

where F represents the input frequencies, is characterized by an offset, b, a 'knee' parameter, k (which, if not equal to zero, adds a bend to the aperiodic signal), and the exponent or slope, X. We chose to fit the power spectrum with $k = 0$ between 9-25 Hz as this gave a good fit with low error and high R squared values. We averaged the exponents and error values of all LFP traces for each animal.

Finally, we quantified bursts of hyperexcitable activity by the automated detection of episodes of high β-σ (9-25 Hz) signal strength as for up state detection, but with the added restraint that the episode should be at least 4 times as long as an average up state of control animals (4*0.85 s). In this way, we ensured that the labelled event was not a physiologically correct up state. EEG signals were evaluated for the presence of β oscillations in the same way. Hypersynchronous peaks were automatically detected as episodes of high γ (40-100 Hz) signal strength (again as described for up state detection) of a duration between 30 and 300 ms, with a downward slope of at least 10 mV/s (calculated from the peak till the half maximum of the peak) and an amplitude of at least 0.3 mV. Timing of these events were correlated with timing of up states in the opposite, control hemisphere. Values were averaged per animal.

The EEG data from the behaving mice were used to score sleep phases by an adaptation of the algorithm termed SCOPRISM (Bastianini et al. 2014) and our code is available at https://github.com/DidiLamers/PCDH19_sleepscoring.

In brief, epochs of 4 seconds were scored based on the RMS of the EMG signal to distinguish wake from sleep. The identification of REM and NREM sleep segments was performed by computing the ratio of the EEG spectral power ratio in the θ (6-9 Hz) to the δ (0.5-4 Hz) band: NREM (slow wave sleep) is characterized by high δ power and relatively lower θ power. Scoring was then refined based on scoring results of surrounding epochs. Data were cleared by artefacts by ignoring all epochs with an EEG or EMG value above a manually set threshold (usually set to 300 µV).

Data analyses: 2 photon imaging

Calcium imaging data were analysed using custom written software in MATLAB (Cozzolino et al., 2020), and code is available on Github: https://github.com/DidiLamers/PCDH19_CalciumImaging). In brief, images were binned 2*2 and the time series representing the fluorescence fluctuation for each pixel was computed as

$$\Delta F(x,y,t)/F_0 = \frac{f(x,y,t) - \langle f(x,y)\rangle}{\langle f(x,y)\rangle}$$

with $f(x,y,t)$ representing the fluorescence signal of that pixel and $\langle f(x,y)\rangle$ the median fluorescence. We then used the statistics of the $\Delta F(x,y,t)/F_0$ signal to create a binarized image. In the absence of any calcium activity, $\Delta F(x,y,t)/F_0$ will be normally distributed. Calcium activity appears as a tail on the right side of the distribution. We computed the threshold at 2 times the standard deviation of the Gaussian distribution of the $\Delta F(x,y,t)/F_0$ process and pixels of each frame were labelled as either '0' when below threshold or '1' if over threshold. In this way, the binarized stack contains only physiologically relevant events. We added a further restraint by rejecting all isolated pixels.

The binary file was saved and imported in ImageJ, where we set ROIs representing 'green' (expressing EGFP-Cre recombinase and jRGECO1a) or 'red' (expressing jRGECO1a only) cells based on the summed fluorescence signal in the red and green channels. We then counted calcium transients using ImageJ's *Analyze Particles* macro on the binary file in the entire field of view and the 'red' and 'green' cells. These data were used to calculate the transient frequency as well as the percentage of calcium transients occurring during up states in each cell and field of view.

Data analyses: statistics

All statistical analyses were performed in GraphPad Prism 5 software (GraphPad Inc., San Diego, CA). All statistical hypotheses were tested with non-parametric tests. If not otherwise specified, we used a Wilcoxon signed-rank test for paired measurements (i.e. to compare the two hemispheres) and a Mann Whitney test to compare two experimental groups.

References

S. Bastianini, C. Berteotti, A. Gabrielli, F. Del Vecchio, R. Amici, C. Alexandre, T. E. Scammell, M. Gazea, M. Kimura, V. Lo Martire, A. Silvani, and G. Zoccoli. SCOPRISM: A new algorithm for automatic sleep scoring in mice. Journal of Neuroscience Methods, 235:277_284, 2014.

H. Bokil, P. Andrews, J. E. Kulkarni, S. Mehta, and P. Mitra. Chronux: A Platform for Analyzing Neural Signals. Journal of neuroscience methods, 192(1):146_151, 2010.

Cozzolino O, Sicca F, Paoli E, Trovato F, Santorelli FM, Ratto GM, Marchese M. Cells Evolution of Epileptiform Activity in Zebrafish by Statistical-Based Integration of Electrophysiology and 2-Photon Ca^{2+} Imaging. 2020 Mar 21;9(3):769. doi: 10.3390/cells9030769.

Esser SK, Hill SL, Tononi G. Sleep homeostasis and cortical synchronization: I. Modeling the effects of synaptic strength on sleep slow waves. Sleep. 2007 Dec;30(12):1617-30. doi: 10.1093/sleep/30.12.1617.

Donoghue T, Haller M, Peterson EJ, Varma P, Sebastian P, Gao R, Noto T, Lara AH, Wallis JD, Knight RT, Shestyuk A, Voytek B. Parameterizing neural power spectra into periodic and aperiodic

components. Nat Neurosci. 2020 Dec;23(12):1655-1665. doi: 10.1038/s41593-020-00744-x. Epub 2020 Nov 23. PMID: 33230329; PMCID: PMC8106550.

Petrucco L, Pracucci E, Brondi M, Ratto GM, Landi S. Epileptiform activity in the mouse visual cortex interferes with cortical processing in connected areas. Sci. Rep. 2017 Jan 10;7:40054. doi: 10.1038/srep40054.

Quiroga RQ, Nadasdy Z, Ben-Shaul Y. Unsupervised spike detection and sorting with wavelets and superparamagnetic clustering. Neural Comput. 2004 Aug;16(8):1661-87. doi: 10.1162/089976604774201631.

Trovato F, Parra R, Pracucci E, Landi S, Cozzolino O, Nardi G, Cruciani F, Pillai V, Mosti L, Cwetsch AW, Cancedda L, Gritti L, Sala C, Verpelli C, Maset A, Lodovichi C, Ratto GM. Modelling genetic mosaicism of neurodevelopmental disorders in vivo by a Cre-amplifying fluorescent reporter. Nat Commun. 2020 Dec 3;11(1):6194. doi: 10.1038/s41467-020-19864-w.

Vyazovskiy VV, Riedner BA, Cirelli C, Tononi G. Sleep homeostasis and cortical synchronization: II. A local field potential study of sleep slow waves in the rat. Sleep. 2007 Dec;30(12):1631-42. doi: 10.1093/sleep/30.12.1631.

Supplementary Information

Supplementary Figure 1

Generation of the PCDH19 mosaic model

All experiments were performed on a conditional mouse line where exon 3 of PCDH19 is flanked by LoxP sequences (figure S1A). We induced a patch of Cre-mediated recombination by a focal injection of an AAV expressing EGFP-Cre. To confirm that PCDH19 expression was reduced, we resorted to a quantitative Western Blot (WB). We found that PCDH19 protein expression is reduced in the injected hemisphere compared to that of EGFP injected control mice (figure S1B; P=0.003). This demonstrates that, even though Cre removes only exon 3, the entire protein is missing. It is likely that excision of exon 3 causes a frameshift and premature stop codon in the gene upon which the mRNA is degraded by nonsense-mediated decay. Immunohistochemistry (IHC) for Cre-recombinase shows that at the injection site we have obtained a 'salt-and-pepper' like mosaicism since not all neurons expresses Cre (figure S1C). Further evidence for this notion is provided by an In Situ Hybridization (ISH) for exon 1 of PCDH19 showing that the EGFP-Cre recombinase injection strongly reduces the staining in floxed mice, but not in non-floxed littermates (figure S1D). We therefore conclude that upon Cre-mediated recombination of exon 3, mRNA expression of exon 1 is also reduced. The ISH confirms previous studies demonstrating that PCDH19 is mainly expressed in layers II/III and layer V of the cortex (Dibbens *et al.*, 2008; Pederick *et al.*, 2016; Hayashi et al., 2017). Within these cortical layers PCDH19 is not present in every cell (Krishna-K *et al.*, 2011; figure S1D bottom right). We therefore conclude that Cre recombinase injection causes a cellular mosaicism.

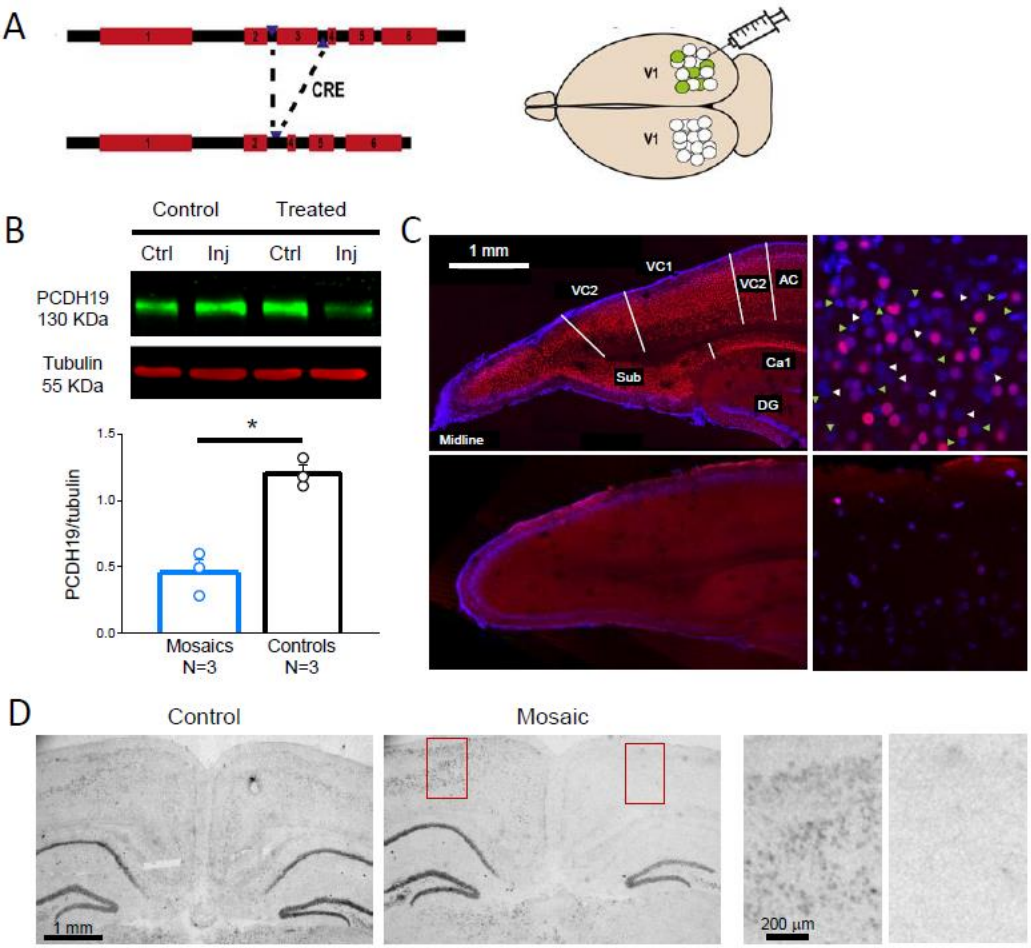

Supplementary figure S1: Focal model of mosaic PCDH19 expression. A) Creation of the mouse model. Exon 3 of the PCDH19 gene was placed between LoxP sites, allowing for excision of the exon upon introduction of Cre recombinase. **B**) Quantitative WB confirms a reduction in PCDH19 protein expression in the hemisphere injected with the Cre vector (in blue) versus control (floxed mice injected with the EGFP vector, in black) by about half (average PCDH19/tubulin value of injected hemisphere/control hemisphere of 0.46 ± 0.09 in 'Mosaics' versus 1.20 ± 0.06 for controls, * P<0.005 t-test. Top image shows the WB for two example animals: one control and one mosaic. Staining for PCDH19 (in green) was normalized by the expression of housekeeping gene Tubulin (in red) and values for the injected hemisphere (inj) were normalized by values for the control (ctrl) hemisphere. **C**) IHC of Cre recombinase (in red) in the injected (top) and control (bottom) hemisphere of an EGFP-Cre recombinase injected floxed mouse. Cre positive (green arrows) and negative (white arrows) cells are visible in the higher magnification image (on the right) in the injected hemisphere, with no Cre present in the control hemisphere. V1: primary visualcortex, V2: secondary visual cortex, DG: dentate gyrus, Sub: subiculum, AC: auditory cortex. Section located 3.5 mm posterior to bregma. **D**) ISH for PCDH19 exon 1 of an injected non-floxed mouse (left) and an injected floxed littermate (right). The expression of exon 1 is strongly reduced in the cortex and in part of the hippocampus of the injected hemisphere of the floxed, but not of the control mouse. The doted rectangles are drawn in correspondence of the magnified insets on the right. Section located 2.5 mm posterior to bregma. All mice in this figure were injected at P1 and sacrificed as adults.

Supplementary Figure 2. SWA characterization

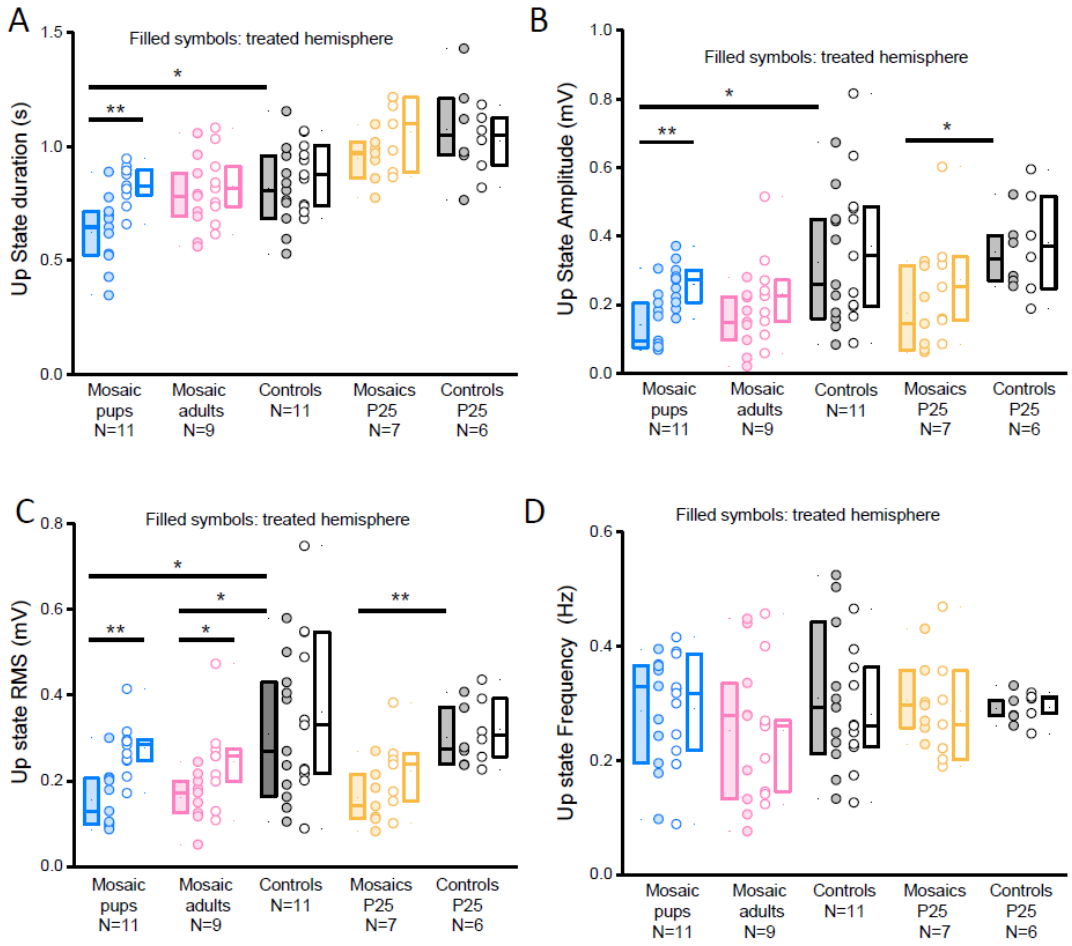

Supplementary figure S2: Up state characteristics are affected by PCDH19 mosaicism. Up state duration **A**), amplitude **B**), and RMS strength **C**) are all reduced in PCDH19 mosaic tissue, while their frequency **D**) is not altered. All graphs represent box plots with whiskers of minimum and maximum values of all three experimental groups, while dots represent the average value per animal with the values of the two hemispheres connected by lines. Significant differences are indicated with asterisks (** P<0.005, * P<0.05; Wilcoxon signed-rank test for paired measurements; Mann Whitney test for non-paired). US duration is significantly reduced in the injected hemisphere of Mosaic pups compared to their control hemisphere (P<0.001) and to the injected hemisphere of Control animals (P<0.03). US amplitude is similarly reduced in the injected hemisphere of Mosaic pups (P<0.001 compared to the control hemisphere and P<0.02 compared to the injected hemisphere of Controls). Also, the injected hemisphere of mice recorded at P25 displays a reduced US amplitude, though only compared to the injected hemisphere of Control animals (P<0.04). RMS signal strength of up states is reduced in Mosaic pups (injected hemisphere versus control hemisphere: P<0.001, injected hemisphere of Mosaics versus injected hemisphere of Controls: P<0.02), Mosaic Adults (injected versus control hemisphere: P<0.02; injected hemisphere of Mosaic adults versus that of Controls: P<0.05) and mice recorded at P25 (injected hemisphere of Mosaic P25 animals versus that of Controls: P<0.005). US frequency is unaltered in all cases.

Supplementary Figure 3. Estimate of the E:I ratio by means of the study of the slope of the LFP power spectra. Changes in the E:I ratio after GABA superfusion.

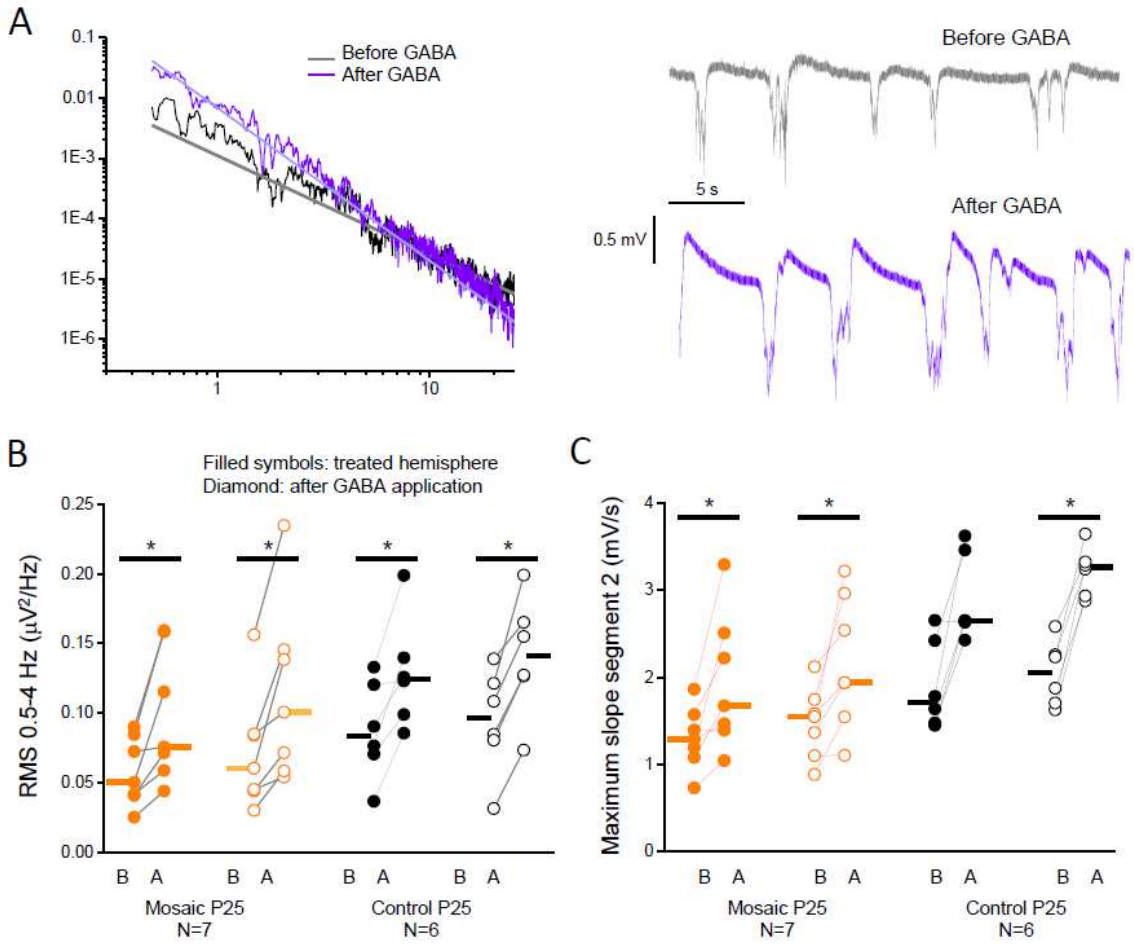

Supplementary figure S3: PCDH19 mosaic animals have an increased excitation to inhibition ratio. A) Example power spectrum of a control animal recorded at P25 (black line) and the exponential fit (thick line) computed with the FOOF algorithm. After GABA application, the power spectra changed as shown by the magenta line and its exponential fit (thick magenta line). This spectrum is steeper (an exponent of 2.54 versus 1.64 before GABA application). The Root Mean Square Error of both fits is 0.12 and the R^2 is 0.95 (before GABA) and 0.97 (after GABA). The corresponding LFP traces are shown to the right (before GABA application in grey, after in magenta). Note the large amplitude slow waves after GABA application. **B**) Bar plots representing median RMS strength in the 0.5-4 Hz range (left) and the US slope (right). Dot plots display the values of each animal, with lines connecting the values before (B) and after (A) GABA application. In red are the mosaic animals recorded at P25, in black their controls. Open dots represent the injected hemisphere, closed ones the control hemisphere. GABA application significantly increases SWA (the RMS in the 0.5-4 Hz range; before versus after GABA application of the injected hemisphere of Mosaics P=0.02, their control hemisphere P<0.02, the injected hemisphere of Controls P<0.03, and the control hemisphere of Controls: P<0.03) as well as the slope of USs **(C)** (before versus after GABA application of the injected hemisphere of Mosaics P<0.03, their control hemisphere P<0.02, the injected hemisphere of Controls P<0.06, and the control hemisphere of Controls: P<0.03).

Supplementary Table 1

Since PCDH19 Epilepsy primarily affects females, we tested whether there was a difference in phenotype between male and female mice. In agreement with the hypothesis that a mosaic PCDH19 expression causes the disease, we found that male and female mice showed a similar reduction in δ oscillatory strength (figure 3B; inset). Since we recorded only four males, the difference was not significant for males (P=0.1) but it was for females (P=0.02). Note that none of the analyses that we performed on the LFP data showed differences between males and females in the 'Mosaic Pups' experimental group. In all the upcoming graphs the values of male and female mice were therefore pooled.

	Male (N=4) treated hemisphere	*Male (N=4) control hemisphere*	*Female (N=7) treated hemisphere*	*Female (N=7) control hemisphere*
RMS 0.5-4 Hz (mV)	0.045 ± 0.010	0.092 ± 0.030	0.046 ± 0.032	0.088 ± 0.032
Up State Duration (s)	0.69 ± 0.04	0.83 ± 0.04	0.59 ± 0.19	0.83 ± 0.11
Up State Amplitude (mV)	0.16 ± 0.06	0.28 ± 0.02	0.13 ± 0.08	0.25 ± 0.08
Up State RMS (mV)	0.18 ± 0.052	0.28 ± 0.034	0.14 ± 0.077	0.28 ± 0.08
Up State Frequency (Hz)	0.33 ± 0.092	0.34 ± 0.088	0.26 ± 0.101	0.27 ± 0.101
Maximum Up State slope segment 2 (mV/s)	0.95 ± 0.34	2.08 ± 0.70	0.99 ± 0.66	2.22 ± 0.82
Unit Frequency (Hz)	1.06 ± 0.24	5.90 ± 3.02	1.36 ± 0.48	3.30 ± 1.80
Units in Up State (%)	50.4 ± 9.8	88.2 ± 8.0	35.9 ± 27.3	61.5 ± 22.0
Slope Power Spectrum (exponent)	1.58 ± 0.06	1.90 ± 0.08	1.53 ± 0.37	2.07 ± 0.29

Supplementary table 1: LFP characteristics of 'Mosaic Pups' in males versus females. All values are mean with SD. Males do not show significant differences compared to females and the two experimental groups were therefore pooled.

915 **Supplementary table 2:** Up State slopes are reduced in mosaic mice. All values are mean (mV/s) ±
916 SEM.

917

	Average slope segment 1	*Maximum slope segment 1*	*Average slope segment 2*	*Maximum slope segment 2*
'Mosaic Pups' treated hemisphere	-0.660 ± 0.098	-1.047 ± 0.164	0.595 ± 0.092	0.973 ± 0.165
'Mosaic Pups' control hemisphere	-1.481 ± 0.150	-2.400 ± 0.227	1.298 ± 0.139	2.169 ± 0.222
'Mosaic Adults' treated hemisphere	-0.723 ± 0.088	-1.218 ± 0.164	0.777 ± 0.098	1.296 ± 0.175
'Mosaic Adults' control hemisphere	-1.190 ± 0.154	-2.065 ± 0.252	1.180 ± 0.178	1.977 ± 0.299
'Controls' treated hemisphere	-1.623 ± 0.242	-2.672 ± 0.411	1.340 ± 0.169	2.350 ± 0.305
'Controls' control hemisphere	-1.963 ± 0.301	-3.194 ± 0.494	1.500 ± 0.193	2.773 ± 0.394
'Mosaic P25' treated hemisphere	-0.842 ± 0.078	-1.405 ± 0.145	0.806 ± 0.069	1.304 ± 0.136
'Mosaic P25' control hemisphere	-0.898 ± 0.090	-1.569 ± 0.180	0.844 ± 0.065	1.479 ± 0.155
'Controls P25' treated hemisphere	-1.076 ± 0.118	-1.850 ± 0.209	1.100 ± 0.129	1.904 ± 0.208
'Controls P25' control hemisphere	-1.135 ± 0.048	-1.992 ± 0.121	1.168 ± 0.089	2.047 ± 0.151

918

919

Supplementary table 3: Root Mean Square Error and R^2 of the fit of the power spectra in the 0.5-25 Hz range of our mice with an exponential function (Donoghue *et al.*, 2020). All values show mean ± SEM of all animals in each experimental group.

	RMSE	*R^2*
'Mosaic Pups' treated hemisphere	0.132 ± 0.005	0.914 ± 0.009
'Mosaic Pups' control hemisphere	0.125 ± 0.003	0.953 ± 0.003
'Mosaic Adults' treated hemisphere	0.135 ± 0.004	0.922 ± 0.015
'Mosaic Adults' control hemisphere	0.125 ± 0.003	0.940 ± 0.006
'Controls' treated hemisphere	0.126 ± 0.003	0.951 ± 0.006
'Controls' control hemisphere	0.127 ± 0.004	0.955 ± 0.006
'Mosaic P25' treated hemisphere	0.121 ± 0.004	0.940 ± 0.005
'Mosaic P25' control hemisphere	0.123 ± 0.002	0.944 ± 0.004
'Controls P25' treated hemisphere	0.140 ± 0.011	0.942 ± 0.012
'Controls P25' control hemisphere	0.140 ± 0.010	0.944 ± 0.006

References

Dibbens, L. M. *et al.* X-linked protocadherin 19 mutations cause female-limited epilepsy and cognitive impairment. *Nat. Genet.* **40**, 776–781 (2008).

Donoghue T, Haller M, Peterson EJ, Varma P, Sebastian P, Gao R, Noto T, Lara AH, Wallis JD, Knight RT, Shestyuk A, Voytek B. Parameterizing neural power spectra into periodic and aperiodic components. Nat Neurosci. Dec;23(12):1655-1665 (2020).

Hayashi, S. et al. Loss of X-linked Protocadherin-19 differentially affects the behavior of heterozygous female and hemizygous male mice. Sci. Rep. 7, (2017).

Krishna-K K, Hertel N, Redies C. Cadherin expression in the somatosensory cortex: evidence for a combinatorial molecular code at the single-cell level. Neuroscience Feb 23;175:37-48 (2011).

Pederick *et al.* Pcdh19 Loss-of-Function Increases Neuronal Migration In Vitro but is Dispensable for Brain Development in Mice. *Sci Rep.* **6**:26765 (2016).